A SURVEY OF LOCAL INTERSTELLAR HYDROGEN FROM OAO-2 OBSERVATIONS OF LYMAN ALPHA ABSORPTION

Blair D. Savage
University of Wisconsin
Madison, Wisconsin

Edward B. Jenkins
Princeton University
Princeton, New Jersey

ABSTRACT

The Wisconsin far-ultraviolet spectrometer aboard OAO-2 observed the wavelength region near 1216 Å for 69 stars of spectral type B2 or earlier. From the strength of the observed interstellar L_α absorption, atomic hydrogen column densities were derived over distances averaging 300 pc away from the sun. Measurements of the equivalent widths of this absorption were found to be inappropriate for deducing column densities because of the blending of nearby strong stellar lines by the 12 Å wide instrumental profile of the OAO. Instead, the OAO data were compared to synthetic ultraviolet spectra, originally derived from earlier higher resolution rocket observations, which were computer processed to simulate the effects of absorption by different amounts of hydrogen followed by the instrumental blending.

An average volume density $n_H = 0.6$ atoms cm^{-3} was derived using all the stars. For stars nearer the sun ($r<140$ pc) we obtained $n_H = 0.25$ atoms cm^{-3}. The fact that no stars were observed much beyond 1 kpc precludes our obtaining any general information on large-scale galactic structure. However there is evidence for a pronounced enrichment of gas toward a number of stars in Scorpius, and a general deficiency seems to exist in the $180° < l^{II} < 270°$ sector. A comparison of L_α column densities

to those derived from observations of 21-cm emission shows a very poor correlation, which demonstrates the importance of the unavoidable differences in sampling geometry. The L_α column densities correlated reasonably well with D line, H and K line and color excess measurements for the respective stars, and the average ratios $\langle N_{NaI}/N_{HI}\rangle = 3.5 \times 10^{-9}$, $\langle N_{CaII}/N_{HI}\rangle = 2.5 \times 10^{-9}$ and $\langle N_H/E(B-V)\rangle = 5 \times 10^{21}$ atoms $cm^{-2}mag^{-1}$ were obtained. For assumed ionization equilibrium constants and a model for the interstellar medium, we find the observed ratios imply the total abundances $\langle Na/H\rangle = 2.3 \times 10^{-7}$ and $\langle Ca/H\rangle = 6.8 \times 10^{-9}$. For a very recent grain model we derive $\langle \rho_{HI}/\rho_{dust}\rangle \simeq 100$ from the $\langle N_H/E(B-V)\rangle$ relation.

I. INTRODUCTION

It has long been recognized that ultraviolet observations from space observatories can provide important new information on the interstellar gas and dust (Spitzer and Zabriskie 1959; Code 1960). The successful launch and operation of the second Orbiting Astronomical Observatory (OAO-2) (Code, Houck, McNall, Bless and Lillie 1970) has demonstrated that stellar space observatories can be designed to yield high-quality astronomical data for long periods of time. OAO-2 was launched on December 7, 1968, and at the time of writing (~2-1/2 years later) continues to collect high-quality scientific data. In this paper we will report on observations of the absorption from the interstellar Lyman alpha (L_α) line of atomic hydrogen at 1215.7 Å made by OAO-2. Other papers have dealt with OAO-2 observations of interstellar dust (Bless and Savage 1970, 1972).

Interstellar L_α absorption was first observed with sounding-rocket instrumentation by Morton (1967) in the far ultraviolet spectra of O and B type stars in Orion (see also Jenkins and Morton 1967). Since that first observation, sounding rockets have recorded the L_α line in approximately 20 stars. Reviews of these rocket observations and their implications have been given by Carruthers (1970a) and Jenkins (1970a). The primary conclusion which has been drawn from these observations is that the local interstellar hydrogen density is of the order of 0.1 atom cm^{-3} instead of the 0.7 atom cm^{-3} generally quoted by 21-cm observers (Kerr and Westerhout 1965). In the case of the rocket data the coverage of the sky has been small and therefore these early observations can not be considered as a general survey of the neutral hydrogen near the sun. However, these data have been very important because they have provided

an independent means of obtaining information on neutral interstellar hydrogen.

The short wavelength spectrometer in the University of Wisconsin experimental package on board OAO-2 has observed a large number of stars of type B2 or earlier in the spectral region 1050-1800 Å. For such stars the stellar L_α line is in most cases narrow enough to reside within the highly saturated core of the interstellar L_α profile. The distribution in galactic latitude and longitude of the stars observed is shown in Figure 6. Most stars are within 1000 pc of the Sun and are located near the plane of the galaxy. These new data provide a fairly representative sample of the local interstellar hydrogen.

A preliminary discussion of the OAO L_α data was given by Savage and Code (1970). In that analysis it was recognized that the relatively low resolution of the spectral scans obtained by the OAO produced a blending of the interstellar L_α line with adjacent stellar lines. The equivalent widths reported by Savage and Code were for the blend of stellar and interstellar lines near 1216 Å. This blend equivalent width was used to obtain an upper limit to the hydrogen column density. For many stars the OAO blended equivalent widths were significantly larger (2 to 3 times) than the reported rocket L_α equivalent widths. In contrast, for other cases there was a fair agreement between the OAO blended equivalent widths and the rocket L_α equivalent widths. Since that preliminary OAO report, a large effort has gone toward trying to understand the apparent differences between the OAO data and the rocket data and toward developing a method which corrects for the line blending in the OAO data. In this paper we present the results of this investigation.

II. OBSERVATIONS

The OAO L_α observations were obtained with an objective grating scanning spectrometer having an effective collecting area of 265 cm^2. Starlight was incident on a plane reflecting grating with 300 lines/mm and the first order dispersed light was focused by a parabolic mirror back through a hole in the center of the grating. Behind the grating, a slit having a width of 10 Å was positioned in front of an EMR 541F photomultiplier which contained a LiF window. The spectrum was scanned by a rotation of the grating in discrete wavelength steps of approximately 10 Å. The integration time at each step position for all the L_α data reported here was 8 seconds. In this integration time an unreddened 3rd magnitude B0 star produces approximately 8000 counts in the region of 1200 Å. Typically it was possible to obtain two spectral scans of a star from 1000-2000 Å during one night period of an orbit.

All observations reported here were made at night since the presence of scattered sunlight made the daytime observational material difficult to interpret. For a more detailed description of the OAO instrumentation and observational problems see Code et al. (1970).

Figure 1 shows some typical OAO-2 scans over the wavelengths 1050-1400 Å. We have plotted spectrometer counts vs. wavelength. An individual scan of an early type star would have the appearance of the plot for π Sco (B1 V + B2, m_V = 2.92). In this scan one can easily see spectral features that are primarily due to C III (1175.7 Å, a multiplet of 6 lines), H I (1215.7 Å), and Si IV (1393.8 and 1402.8 Å). In addition, some weaker lines are apparent at 1300 Å and 1335 Å. The line at 1300 Å is produced by a multiplet from an excited level of Si III (lines between 1294.5 and 1303.3 Å) combined with the weak O I interstellar line at 1302.2 Å. The line at 1335 Å is due to a combination of stellar and interstellar C II (1334.5 and 1335.7 Å). These line identifications were made with reference to higher resolution rocket spectra of the Princeton group (Bohlin 1970).

The wavelength scale for the OAO data was established through a comparison of OAO data and higher resolution rocket data degraded to the OAO instrumental resolution. The presence of the strong stellar lines makes such a comparison possible (see Figure 1). It was found that the number of Angstroms per spectrometer step depended on the direction of the scan (because of mechanical backlash), the wavelength and the incident angle.

When more than one spectral scan was obtained for an object, a detailed spectrum could be produced by combining scans. In Figure 1 we have combined two scans of the star τ Sco (B0 V, m_V = 2.83) and also four scans of the star δ Sco (B0.5 IV, m_V = 2.32). These observations were obtained by utilizing the satellite's bore-sighted startracker. With this startracker it was possible to make a scan, change the incident angle by 0.25 arc min (which corresponds approximately to a 2.5 Å shift in the spectrum), and then make another scan. If this process were continued one could produce a composite spectral scan similar to that for δ Sco shown in Figure 1. However, only a few stars were observed using this technique to fill in the data between the 10 Å stepping interval of the scanner. In general we combined two or more totally independent scans and shifted them in wavelength until a reasonable wavelength alignment was obtained. In fortunate situations this procedure led to a significant gain in information about the detailed shape of the spectrum. In other cases the data points simply all coincided.

The OAO spectrometer records a background signal which is a combination of thermal dark counts, counts due to charged

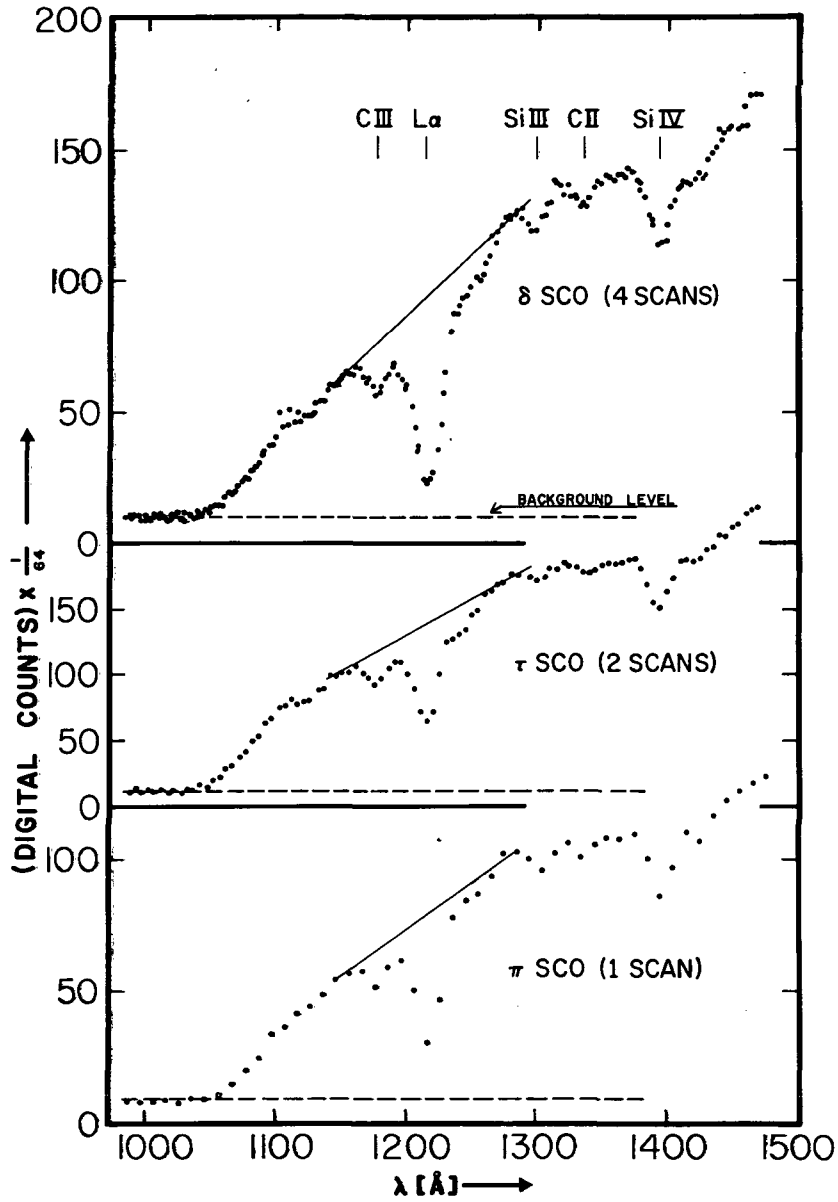

Figure 1.—OAO-2 spectrometer scans of the stars δ Sco (B0.5 IV), τ Sco (B0 V) and π Sco (B1 V + B2). We have plotted raw digital counts vs. wavelength. The 1/64 multiplier for the digital counts is due to a scaler in the OAO electronics. The plot for π Sco illustrates an individual scan. The plots for τ Sco and δ Sco are a composite of 2 and 4 scans, respectively. More frequent sampling than the spectrometer's 10 Å stepping interval was accomplished by controlled offsets in incident angle provided by the spacecraft's bore-sighted startracker. The dashed line represents the extrapolated background level.

energetic particles, sky background light, and scattered light in the optical system. The background due to charged particles from the radiation belts is usually unimportant (for 8-second integration times) except at those times when the satellite passes through the South Atlantic radiation anomaly. In general, astronomical observations were not carried out during this period of time. The scattered light contribution dominates over the other sources of background for O and B type stars brighter than approximately $m_V = 2$. The scattering is undoubtedly from the grating and dust elsewhere in the optical system. The sky background light is mainly resonance scattered L_α from hydrogen in the earth's geocorona. The net background due to all the above mentioned effects can be measured by observing an object shortward of the LiF cutoff of the photomultiplier. In the data illustrated in Figure 1 one can see that for $\lambda<1050$ Å (the LiF cutoff) the counts level off to a constant background level. For the purpose of obtaining L_α line profiles we have assumed that the background level measured at $\lambda<1050$ Å can be extrapolated as a constant background level for wavelengths greater than 1050 Å (see dashed lines in Figure 1). This assumption would have been invalid if some of the various background contributions were wavelength dependent or time dependent. A number of spectral scans of just the dark sky existed which demonstrate that the sky background is essentially constant with wavelength. We feel it is reasonable to assume that the scattered light contribution to the measured background is also wavelength independent. Since for most of the observational material presented in this paper the background is small compared to the observed signal at 1200 Å, the relative uncertainty in the derived intensity will be negligible. However, for stars faint in the ultraviolet the background can be comparable in size to the signal being measured at 1200 Å. Under this situation an uncertainty in the background correction can produce a large uncertainty in the derived intensity. It is this uncertain background correction for faint objects and not counting statistics that limit the instrument for L_α studies to O and B type stars brighter than about $m_V = 5$.

The data in Figure 1 illustrate the reproducibility of the OAO spectrometer observations. In general, spectral scans agree to within an uncertainty governed by photon statistics. Spectral scans of the same objects made two years apart have been compared, and typically they are identical to within 2 to 3%.

Much of the analysis which follows relies upon a detailed fitting of the OAO scanner data to reconstructions of prototype stellar spectra whose resolutions have been degraded. To accomplish this comparison one must know the shape of the

scanner's instrumental slit profile. This profile was derived from OAO observations of zero-order star images and from spectral scans of the relatively narrow He II (1640.4 Å) emission line in the star ζ Pup (O5 f, m_V = 2.25). Rocket observations of this line by one of us (EBJ) show its intrinsic width to be approximately 4 Å. The zero-order image data were used to establish the shape of the instrumental profile while observations of the He II emission line were used to determine width of the profile. A small correction was made for the finite width of the He II line. The derived function has an approximate Gaussian shape with a full width at half intensity of 12 Å. When this function was used to degrade higher resolution rocket spectra, a good agreement was obtained between the OAO scans and degraded rocket observations (see Figure 2). These comparisons will be discussed in detail in § III.

III. DERIVATION OF COLUMN DENSITIES

a) Preliminary Considerations

As mentioned earlier, some equivalent widths reported by Savage and Code (1970) differed significantly from those of the earlier rocket investigators. It was not clear at that time to what degree errors in either case could be attributed to (a) faulty measurements, (b) an improper estimate of the stellar continuum level on either side of 1216 Å or (c) confusion of the L_α profile with nearby stellar absorptions. We shall briefly review our conclusions on these possibilities and show how they influence our approach in the reduction of the OAO data presented here.

In spite of the measurement problems discussed in the previous section, the photometric accuracy of the OAO photoelectric scans is generally more trustworthy than that of the rocket spectra recorded on film. Uncertainties from film grain noise, errors in the film's characteristic curve and ambiguous intensities below the film's threshold must all be recognized as possible sources of error in the raw data from many of the rocket observations. On the other hand, the rocket spectra clearly resolve wavelength intervals significantly smaller than the width of the L_α profile, and we depend upon our ability to see this finer structure to answer questions about the possible sources of error (b) and (c) mentioned earlier.

A necessary (but not sufficient) test of the reliability of the OAO and rocket data is a comparison of the two after the rocket spectra have been convolved with the OAO instrumental profile. It is encouraging to see in Figure 2 that there is a surprisingly good agreement between the independently derived spectra. Figure 2 shows the references where the origi-

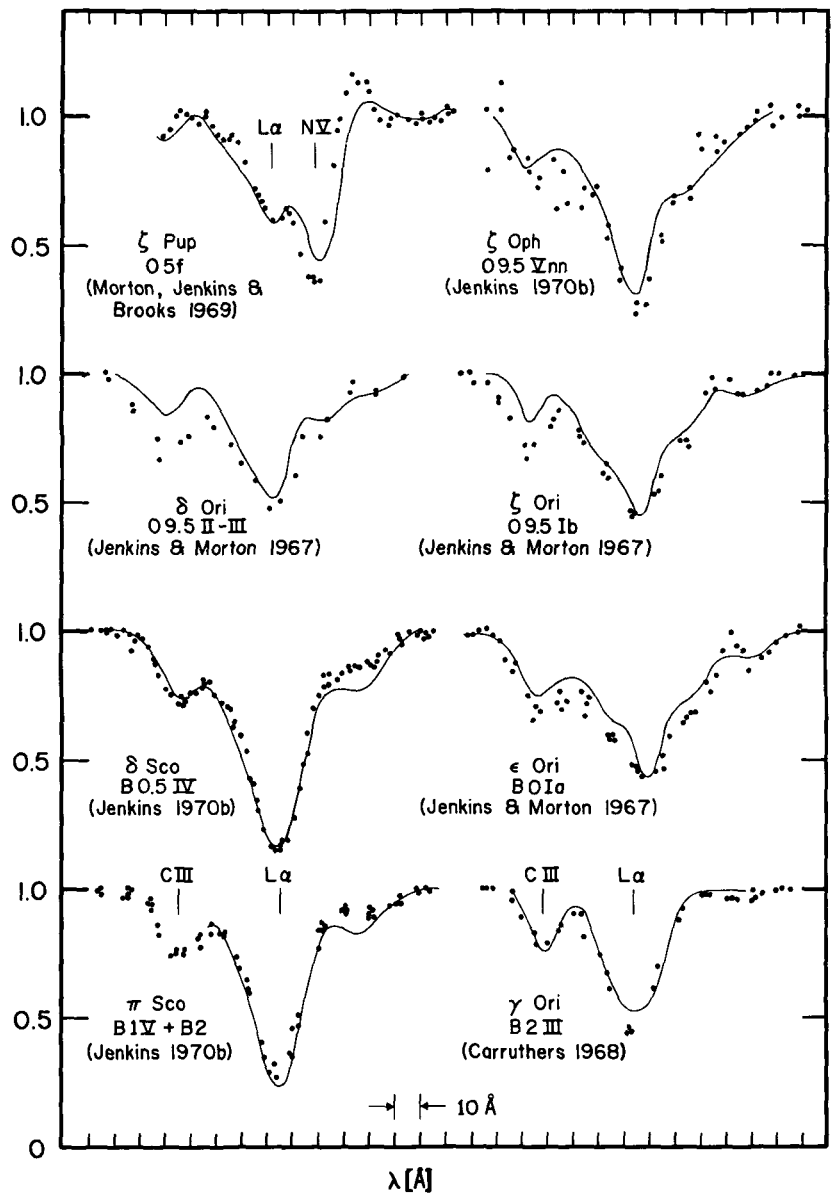

Figure 2.—A comparison of OAO data (dots) with high resolution rocket spectra which have been smoothed by the OAO instrumental profile (curves). Both the OAO and rocket spectra have been renormalized to make the apparent continuum level relatively flat at 1.0 (for the rocket spectrum of δ Sco, this operation is demonstrated in the change from Fig. 4a to 4b).

nal rocket spectra were first recorded. The most serious difference between rocket data and OAO data shown in this figure is seen in ζ Pup. In this case both the emission and absorption components of N V look somewhat different, although the match in the core of the L_α line is good. For this star the rocket intensity calibration may be somewhat in error for the strong emission of the N V line. The slight difference in the core of the L_α line for the γ Ori comparison can probably be understood in terms of too much smoothing of the rocket observation. In the convolution of the rocket data with the OAO slit function we did not allow for the finite resolution of the rocket data. The rocket spectrum of γ Ori was of slightly lower resolution (~3 Å) than the other rocket spectra used. In the case of δ Sco and π Sco it appears that atmospheric O_2 absorption could produce the difference between the OAO and rocket spectra at 1240 Å. One would expect a slightly weaker feature also to occur at 1206 Å (Watanabe, Zelikoff and Inn 1953). The only arbitrary adjustment which was applied to force a correspondence for the profiles in Figure 2 was a multiplication of each spectrum by a smoothly varying function which made the overall height of the continuum nearly level over the complete wavelength span. This renormalization compensated for any sloping trend in the stellar output and differences in each of the instrumental sensitivities versus wavelength. An illustration of this procedure is shown in the transformation of the rocket spectrum of δ Sco between Figures 4a and 4b.

Figure 2 makes it very clear that for these stars previous differences in column densities from OAO and rocket data cannot be attributed to any fundamental disagreement in the recorded information. In trying to explain why many of the rocket investigations revealed significantly lower column densities than their own, Savage and Code (1970) suggested the possibility that their predecessors had failed to account for the depression of the true continuum level by the broad damping wings in the L_α profile, and the rocket equivalent widths were measured under continua drawn systematically too low. Later, Jenkins (1971) reanalyzed the Princeton rocket L_α data for δ, ε and ζ Ori by evaluating the goodness of fit of the observed profiles with theoretical absorption profiles as the hydrogen density and continuum height were both allowed to vary as free parameters. Jenkins pointed out that unless a careful reduction procedure is used, rocket column densities could be subject to errors. Nonetheless, the fact that Jenkins still found much lower column densities for the Orion stars than those of Savage and Code, together with preparations for the work presented here, made it clear that when interstellar column densities were not very large, a principal contribution to the measured equivalent widths in the OAO absorptions recorded

near 1215 Å came from neighboring stellar lines blended in with the L_α absorption.

b) Derivation of N_H

The aforementioned difficulties associated with OAO equivalent width determinations forced us to consider alternate criteria for establishing hydrogen column densities. The following approach was adopted for the analysis of the OAO data. The stars shown in Figures 2 and 3, whose spectra were observed at good resolution by rockets, were selected as prototypes for the analysis of stars of identical or nearly the same spectral type observed by the OAO.

The actual column densities N_a (atoms cm^{-2}) to these stars were either taken from Jenkins' (1971) analysis or evaluated using a somewhat simpler technique suggested in his article. A reconstruction of the appearance of a spectrum in the absence of any absorption by atomic hydrogen was produced by multiplying the observed spectrum by exp $(+\tau)$, where the optical depth τ equaled 4.26×10^{-20} $atom^{-1}$ cm^2 $Å^2$ N_a $(\lambda-\lambda_0)^{-2}$ (Jenkins 1970a, 1971). Near the line core at λ_0, where excessive magnification of small errors would occur, the flux was assumed to be a straight line joining the reconstructed spectrum on either side. Figure 3 shows each prototype spectrum with and without interstellar absorption. One can see in this figure that the nearest strong stellar lines, Si III (1206.5 Å) and N V (1240 Å), are often a major source of line blending for the L_α profile and contribute to varying degrees in the different spectral types exhibited. Occasionally these lines show significant negative velocity shifts. For δ Sco (B0.5 IV), π Sco (B1 V + B2) and γ Ori (B2 III), Si III is the major source of blending, while for ζ Oph (O9.5 Vnn), δ Ori (O9.5 II-III), ζ Ori (O9.5 Ib) and ε Ori (B0 Ia), both Si III and N V contribute to the line blending. N V is a very strong component in ζ Pup (O5 f).

The next step consisted of generating a set of synthetic OAO spectra for these stars for various trial column densities N_t. A substitution of different values for N_t into the equation for τ and multiplication of each spectrum by exp $(-\tau)$ produced high resolution versions of the spectra with various amounts of absorption, and these were subsequently smoothed by the OAO slit function. As a final preparation of the curves for matching with the actual data from other stars, these synthetic curves were renormalized so that they all reached the same height in the vicinity of 1160 Å and 1270 Å. Figure 4 illustrates the various stages described for one of the prototype stars, δ Sco (B0.5 IV).

Figure 5 illustrates how the prototype spectra were used to obtain the adopted hydrogen column densities N_H to each OAO

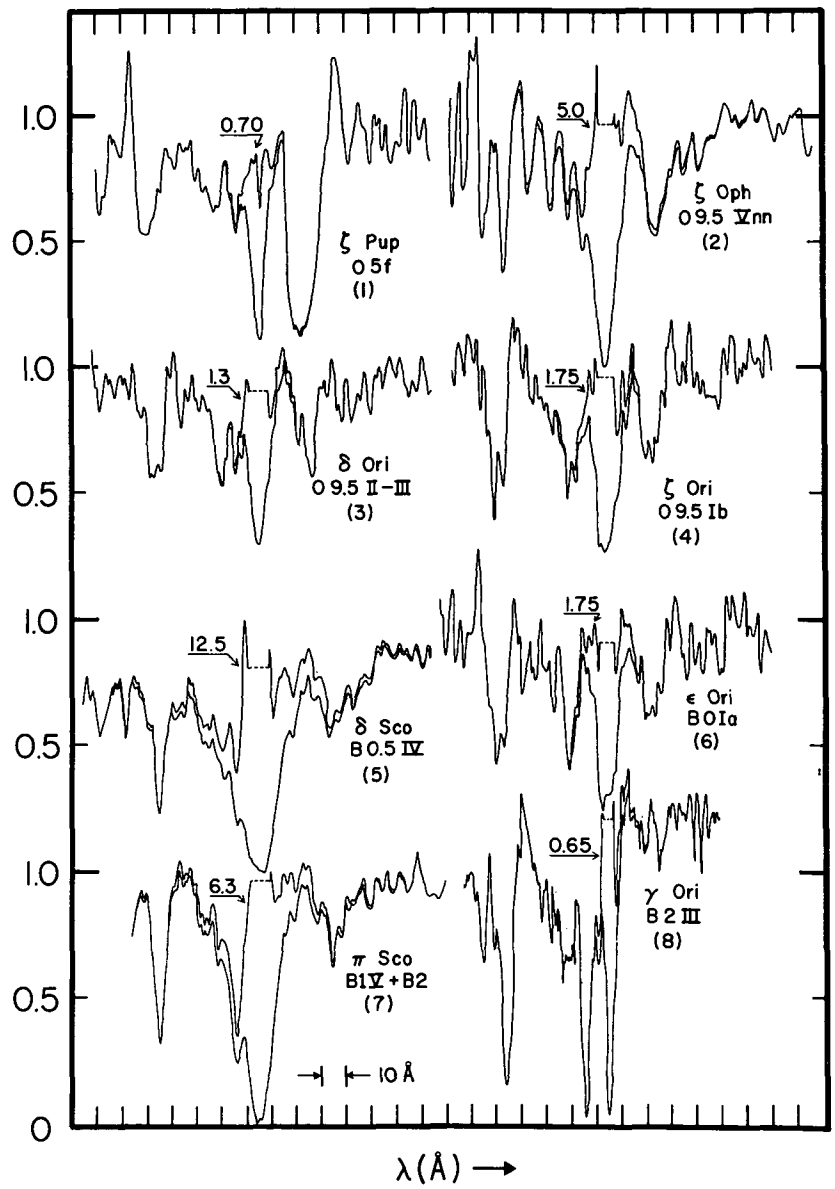

Figure 3.—Eight high resolution (renormalized) rocket spectra chosen for processing into prototype profiles for comparison with the OAO data. The upper curve near L_α represents the original intensity (lower curve) multiplied by exp $[\tau(N_a)]$, where the best estimate for the actual column density N_a to the star is shown in terms of 10^{20} atoms cm^{-2}. The number in parentheses is the code assigned for designating in column 12 of Table 1 which star was used for the derivation of N_H.

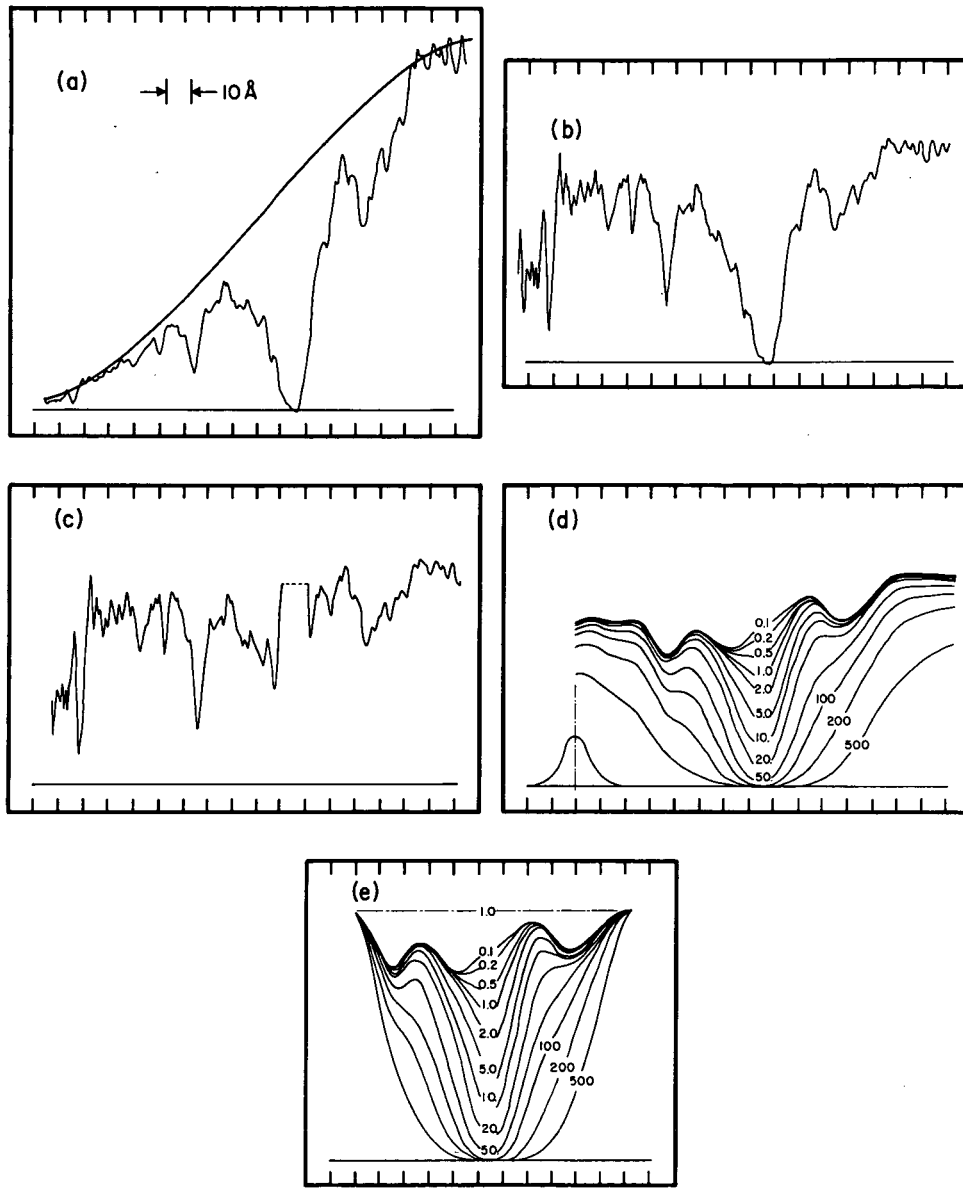

Figure 4.—The steps in preparing a prototype spectrum from an intensity tracing of a rocket spectrum. The spectrum is normalized to the line shown in (a) to give a level spectrum in (b). After multiplication by exp [$\tau(N_a)$], the reconstruction in (c) of the stellar spectrum in the absence of L_α absorption is derived. This profile is multiplied by exp [$-\tau(N_t)$] to simulate the appearance of the spectrum for various column densities N_t. The curves in (d) are the results for the different N_t values (10^{20} atoms cm^{-2}) after a convolution with the instrumental profile shown in the corner of (d). The profiles are ready for comparison with the OAO data after renormalization to a standard height in (e) by a straight line.

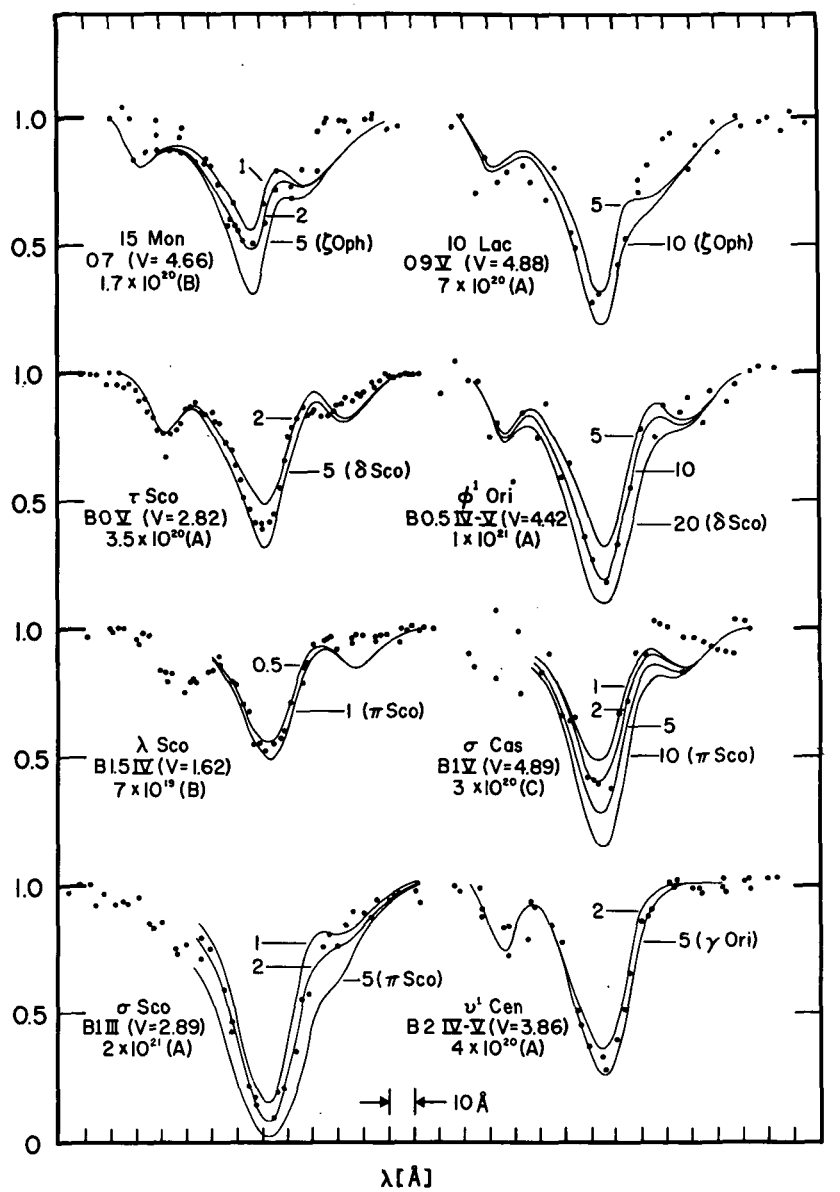

Figure 5.—An illustration of the derivation of hydrogen column densities for eight OAO stars. The dots represent OAO data for the star listed to the left of each profile. The solid lines are prototype spectra for various trial column densities (marked in units of 10^{20} atoms cm^{-2}). The prototype star (indicated in parentheses next to the lowest curve of each set) is the closest match in spectral classification to the OAO star. Below the spectral type and V of each OAO star is shown the adopted N_H and error estimate (A, B or C).

star. The general method of reduction was to choose the prototype star which matched most closely in spectral type and luminosity class the OAO star being analyzed. One then obtained the hydrogen column density by choosing the trial column density that gave the best fit to the OAO data. For example, in the case of the star ϕ^1 Ori (B0.5 IV-V) shown in Figure 5, we used the prototype star δ Sco (B0.5 IV) to obtain the hydrogen column density. As is evident, a trial column density of about 10^{21} atoms cm^{-2} applied to δ Sco would give a good match with the OAO observations of ϕ^1 Ori.

Since in our analysis we employed as prototype spectra only the eight stars shown in Figures 2 and 3, it was not possible always to use a prototype star which matched precisely an OAO star's spectral and luminosity class. For example, in the case of 10 Lac (O9 V) shown in Figure 5 we used the prototype star ζ Oph (O9.5 V) to obtain a column density of 7×10^{20} atoms cm^{-2}. We matched σ Sco (B1 III) with the prototype π Sco (B1 V + B2) to derive $N_H = 2 \times 10^{21}$ atoms cm^{-2}. We shall discuss the possible errors introduced into the final column densities through these unavoidable differences shortly.

The OAO hydrogen column densities as obtained by the above mentioned procedure are contained in Table 1. For each of the stars observed we have listed the following: (1) HD number, (2) name, (3) galactic longitude and (4) latitude (System II), (5) spectral type, (6) V magnitude, (7) B-V color, (8) E(B-V) color excess, (9) distance to star (in pc), (10) OAO hydrogen column density, (11) error and position code (see § IIIc and § IVa), (12) prototype star used to obtain the hydrogen column density (see Fig. 3), (13) mean interstellar space density n_H, (14) 21-cm hydrogen column density N_H (see § IVa), (15) x (see § IVa), (16) simplified model density (see § IVa), (17) Na I and (18) Ca II column densities (see § IVb), and (19) central depth (in percent) of the diffuse feature at 4430 Å. Wherever possible, photometric data for northern stars were taken from Iriarte et al. (1965) and for southern stars from Cousins and Stoy (1963). Spectral types are those given by Lesh (1968) or by Hiltner, Garrison and Schild (1969) for northern and southern objects, respectively. The determination of E(B-V) utilized the intrinsic colors of Johnson (1963). Distances were calculated using the photometric data in the table and absolute visual magnitudes from Blaauw (1963) along with the relation:

$$m_V - M_V = 5 \log r - 5 + 3E(B-V) \quad . \qquad (1)$$

Although there are a number of special cases where other methods could establish more accurate distances, we decided to retain the same system of assigning distances for all our stars in order not to upset the basis for studying regional variations of the hydrogen column density and its correlation

TABLE 1

(1)	(2)	(3)	(4)	(5)	(6)	(7)	(8)	(9)	(10)	(11)	(12)	(13)	(14)†	(15)	(16)	(17)	(18)	(19)
HD	Name	ℓ^{II}	b^{II}	S. T.	V	B-V	E(B-V)	r(pc)	OAO Hydrogen Column Density 10^{20} cm^{-2}	Error Estimate	Comparison Star	Mean Hydrogen Space Density cm^{-3}	21 cm Hydrogen Column Density 10^{20} cm^{-2}	x	Model Density	Na I Column Density 10^{12} cm^{-2}	Ca II Column Density 10^{12} cm^{-2}	Ac (%) λ4430
886	γ Peg	109	-47	B2IV	2.86	-0.21	0.03	180	1.3	B	8	0.23	3.3(1)	0.72	3.0	<0.24(12)		
3360	ζ Cas	121	-9	B2IV	3.66	-0.18	0.06	220	5.0	A	8	0.74		0.24	4.7			3.0(2)
5394	γ Cas	124	-2	B0.5IVe	2.41	-0.11	0.17	180	1.9	B	5	0.34		0.05	3.9	0.21(12)		
10516	φ Per	131	-11	B2Vpe	4.06	-0.04	0.20	160	10.	A	8	2.0	21.(3, 1.0)	0.22	3.4	2.9(4)		
24398	ζ Per	162	-17	B1Ib	2.86	+0.10	0.29	340	12.	A	6, 7	1.1	4.5(4) 9.9(3, 0.6)	0.60	6.3	3.3(4) 2.5(12)	3.2(13)	4.1(2)
24760	ε Per	157	-10	B0.5III	2.89	-0.18	0.10	290	3.0	B	5	0.33		0.35	6.1	1.8(4) 0.6(12)		3.8(2)
24912	ξ Per	160	-13	O7.5	4.06	+0.01	0.33	480	20.	A	1, 2	1.4	9.9(3, 3.5)	0.65	8.6	>7.6(4) 4.1(14) >17.(12)	2.0(13)	3.1(5) 7.2(2)
30614	α Cam	144	+14	O9.5Ia	4.29	+0.03	0.30	830	15.	C	4	0.58	14.(3, 1.5)	0.85	11.			3.4(2)
34816	λ Lep	215	-26	B0.5IV	4.29	-0.25	0.03	540	2.5	V	5	0.15	6.2(1) 8.6(6) 12.(3, 5.4)	0.89	6.0			
35411	η Ori	205	-20	B0.5Vnn	3.32	-0.18	0.10	250	6.0	V	5	0.78	12.(1) 18.(7) 12.(4) 11.(3, 2.7)	0.56	4.8	~3.4(4)		
35439	25 Ori	201	-18	B1Vn	4.95	-0.21	0.05	480	4.0	V	7	0.27	18.(3, 2.3)	0.77	7.3	<0.24(12)		
35468	γ Ori	197	-16	B2III	1.63	-0.21	0.03	110	0.65	V	8	0.19	21.(3, 4.7) 21.(8, 1.4)	0.22	2.4	<0.24(12)	<0.43(12)	
36486	δ Ori	204	-18	O9.5II-III	2.21	-0.21	0.09	340	1.3	V	3	0.12	18.(7) 10.(4) 18.(3, 1.9)	0.63	6.2	0.6(4)		0.2(5) 1.0(2)
36512	υ Ori	210	-19	BOV	4.63	-0.26	0.04	600	3.0	V	5	0.16	8.5(1) 10.(7) 12.(3, 2.1)	0.84	7.8			
36822	ϕ^1 Ori	195	-12	B0.5IV-V	4.42	-0.15	0.13	450	10.	V	5	0.72	24.(3, 0.9) 23.(8, 0.2)	0.60	8.4	2.9(14) 2.8(12)	2.9(13)	
36861	λ Ori	195	-12	O8	3.39	-0.18	0.13	440	11.	V	2	0.81	24.(3, 0.6) 23.(8, 0.5)	0.58	8.3	~4.2(4) 2.6(12) 2.9(14)	2.7(13)	2.0(2)

TABLE 1 (continued)

(1)	(2)	(3)	(4)	(5)	(6)	(7)	(8)	(9)	(10)	(11)	(12)	(13)	(14)†	(15)	(16)	(17)	(18)	(19)
HD	Name	ℓ^{II}	b^{II}	S. T.	V	B-V	E(B-V)	r(pc)	OAO Hydrogen Column Density 10^{20} cm^{-2}	Error Estimate	Comparison Star	Mean Hydrogen Space Density cm^{-3}	21 cm Hydrogen Column Density 10^{20} cm^{-2}	x	Model Density	Na I Column Density 10^{12} cm^{-2}	Ca II Column Density 10^{12} cm^{-2}	Ac (%) λ4430
37022	θ Ori	209	-19	O6p	5.13	+0.04	0.36	870	11.	W	*	0.47	19.(10)	0.86	7.9	1.9(12)	1.8(13)	1.3(9)
-41				O9.5Vp	5.07	-0.09	0.21	650					29.(11)			1.7(12)		1.8(5)
																		7.5(2)
37043	ι Ori	210	-20	O9III	2.76	-0.23	0.08	440	1.5	W	3, 4	0.11	12.(4)	0.76	6.8	<0.74(4)	1.7(13)	0.0(2)
													12.(3, 3.5)			0.54(14)		
																0.65(12)		
37128	ε Ori	205	-17	B0Ia	1.70	-0.19	0.05	360	1.75	W	6	0.16	18.(7)	0.64	6.5	2.1(4)	0.98(13)	-0.1(5)
													14.(4)			1.6(12)		0.0(2)
													18.(3, 3.0)			1.3(14)		
37468	σ Ori	207	-17	O9.5V	3.83	-0.24	0.06	450	5.0	W	2	0.36	18.(7)	0.73	7.3	2.5(4)	0.62(13)	0.0(2)
													18.(3, 4.6)			3.3(14)		
37742	ζ Ori	206	-17	O9.5Ib	1.74	-0.21	0.06	320	1.75	W	4	0.18	18.(7)	0.58	6.0	2.5(4)	0.97(14)	0.5(5)
													18.(3, 4.1)			1.3(14)		1.0(2)
																2.1(12)		
38771	κ Ori	215	-19	B0.5Ia	2.06	-0.18	0.04	470	4.0	W	6	0.28	16.(7)	0.76	7.2	2.3(4)	1.0(14)	2.0(2)
													20.(3, 2.8)			1.5(14)	1.1(13)	
													12.(15, 3.6)			1.4(12)		
40111	139 Tau	184	+1	B1Ib	4.83	-0.07	0.12	1080	8.0	C	6, 7	0.24		0.11	24.		3.6(13)	3.9(5)
																		5.5(2)
44743	β CMa	226	-14	B1II-III	1.98	-0.24	0.00	220	0.2	C	7	0.029	24.(3, 3.0)	0.38	4.6	<0.24(12)		0.4(5)
													20.(8, 1.1)					
47839	15 Mon	203	+2	O7	4.66	-0.24	0.08	900	1.7	B	2	0.061		0.24	19.	0.64(12)		0.9(9)
52089	ε CMa	240	-11	B2II	1.50	-0.21	0.01	180	0.2	C	8	0.036		0.25	3.9			1.0(5)
57060	UW CMa	238	-5	O7f	4.95	-0.15	0.17	910	3.5	A	1, 2	0.12		0.55	18.	3.0(12)	1.6(13)	
66811	ζ Pup	256	-5	O5f	2.25	-0.29	0.03	390	0.7	A	1	0.058		0.23	8.4	<0.24(12)	<0.43(12)	
91316	ρ Leo	235	+53	B1Iab	3.85	-0.13	0.06	750	4.5	A	6, 7	0.19	2.4(1)	1.00	3.8	1.2(4)	1.2(13)	2.8(9)
													5.5(6)			0.76(12)	1.2(14)	2.3(5)
													5.3(15, 1.6)			0.72(14)		
93030	θ Car	290	-5	B0.5Vp	2.75	-0.23	0.05	210	2.5	B	5	0.39		0.13	4.6			
105435	δ Cen	296	+12	B2IVne	2.63	-0.09	0.15	130	1.3	B	8	0.32		0.19	2.8			
106490	δ Cru	298	+4	B2IV	2.82	-0.24	0.00	170	1.5	B	8	0.29		0.08	3.7			
108248	α^1 Cru	300	0	B0.5IV	0.81	-0.25	0.03	110	0.6	C	5, 7	0.18		0.00	2.4			
-49	α^2 Cru			B1V														

TABLE 1 (continued)

(1)	(2)	(3)	(4)	(5)	(6)	(7)	(8)	(9)	(10)	(11)	(12)	(13)	(14)†	(15)	(16)	(17)	(18)	(19)
HD	Name	ℓ^{II}	b^{II}	S. T.	V	B-V	E(B-V)	r(pc)	OAO Hydrogen Column Density 10^{20} cm^{-2}	Error Estimate	Comparison Star	Mean Hydrogen Space Density cm^{-3}	21 cm Hydrogen Column Density 10^{20} cm^{-2}	x-	Model Density	Na I Column Density 10^{12} cm^{-2}	Ca II Column Density 10^{12} cm^{-2}	Ac (%) λ4430
111123	β Cru	302	+3	B0.5III	1.24	-0.24	0.04	150	1.5	B	5	0.32		0.06	3.3			
116658	α Vir	316	+51	B1IV	0.96	-0.25	0.01	100	0.4	B	7	0.13	1.6(1) 6.9(15, 0.5)	0.51	2.0	<0.023(4) <0.062(16)	<0.43(12) 0.040(16)	
118716	ε Cen	310	+9	B1III	2.29	-0.24	0.02	210	0.8	B	7	0.12		0.23	4.5			
120307	ν Cen	314	+20	B2IV	3.40	-0.22	0.02	210	1.2	B	8	0.18	10.(15, 2.5)	0.48	4.2	<0.24(12)		
120324	μ Cen	314	+19	B2IV-Ve	2.97	-0.17	0.07	140	2.0	B	8	0.46	10.(15, 3.0)	0.32	3.0			
121790	υ^1 Cen	315	+16	B2IV-V	3.86	-0.21	0.03	210	4.0	A	8	0.62	6.8(15, 1.8)	0.41	4.3			
122451	β Cen	312	+1	B1III	0.59	-0.22	0.04	90	0.3	C	7	0.11		0.01	2.0			
127381	σ Lup	319	+9	B2III	4.41	-0.20	0.04	380	5.0	A	8	0.43		0.42	7.8			
127972	η Cen	323	+17	B1.5Vn	2.30	-0.21	0.04	110	2.0	B	7	0.59	10.(15, 1.2)	0.23	2.4	<0.24(12)		
129056	α Lup	322	+11	B1.5III	2.29	-0.21	0.04	170	1.5	B	7	0.28	15.(15, 0.8)	0.24	3.6			
132058	β Lup	326	+14	B2III	2.67	-0.21	0.03	170	1.5	B	8	0.28	14.(15, 3.1)	0.29	3.6	<0.24(12)		
132200	κ Cen	327	+15	B2IV	3.12	-0.20	0.04	190	3.0	B	8	0.51	14.(15, 3.8)	0.34	4.0	<0.24(12)		
136298	δ Lup	331	+14	B1.5IV	3.21	-0.22	0.03	230	1.2	C	7	0.17	7.7(15, 2.3)	0.38	4.8	<0.24(12)		
138690	γ Lup	333	+12	B2IV	2.77	-0.20	0.04	150	1.8	B	8	0.39	15. (15, 1.4)	0.22	3.2	<0.24(12)		
141637	1 Sco	346	+22	B1.5Vn	4.69	-0.06	0.16	180	10.	C	7	1.8	8.8(1) 13.(15, 1.0)	0.45	3.6	<2.2(4)		3.4(2)
142669	ρ Sco	345	+18	B2IV-V	3.85	-0.20	0.04	210	5.0	B	8	0.77	15.(15, 3.2)	0.44	4.3			
143018	π Sco	347	+20	B1V, B2	2.92	-0.19	0.06	140	6.3	A	7	1.5	5.8(1) 13.(3, 4.9) 13.(15, 1.0)	0.34	2.9		<0.43(12)	1.8(9)
143275	δ Sco	350	+23	B0.5IV	2.33	-0.10	0.18	170	12.5	A	5	2.4	10.(1) 11.(17) 13.(3, 2.3) 17.(15, 2.3)	0.44	3.4	3.8(4) 1.6(12)	<0.43(12)	1.8(9)
144217	β^1 Sco	353	+24	B0.5V	2.55	-0.08	0.20	160	13.	A	5	2.6	8.8(1) 17.(15, 2.6) 13.(3, 2.3)	0.44	3.3	2.8(4) 1.4(12)	0.70(13) <0.43(12)	4.7(5) 6.7(2)

TABLE 1 (continued)

(1)	(2)	(3)	(4)	(5)	(6)	(7)	(8)	(9)	(10)	(11)	(12)	(13)	(14)†	(15)	(16)	(17)	(18)	(19)
HD	Name	ℓ^{II}	b^{II}	S. T.	V	B-V	E(B-V)	r(pc)	OAO Hydrogen Column Density 10^{20} cm^{-2}	Error Estimate	Comparison Star	Mean Hydrogen Space Density cm^{-3}	21 cm Hydrogen Column Density 10^{20} cm^{-2}	x	Model Density	Na I Column Density 10^{12} cm^{-2}	Ca II Column Density 10^{12} cm^{-2}	Ac (%) λ4430
144470	ω^1 Sco	353	+23	B1V	3.99	-0.04	0.22	240	12.	A	7	1.6	10.(1) 17.(15, 1.6) 13.(3, 2.3)	0.58	4.5	∿2.7(4) 3.3(12)	<0.43(12)	5.6(2)
145502	ν Sco	355	+23	B2V	4.02	+0.04	0.28	140	15.	A	8	3.5	9.0(1) 14.(15, 2.8) 13.(3, 2.9)	0.37	2.9	2.6(4) 3.2(12)		4.8(2)
147165	σ Sco	351	+17	B1III	2.89	+0.14	0.40	160	20.	A	7	4.0	15.(17) 16.(15, 1.0) 16.(3, 1.0)	0.33	3.4	3.4(4) 2.2(12)	0.78(13)	5.7(2)
148703	N Sco	346	+9	B2III	4.23	-0.17	0.07	330	7.0	A	8	0.69	17.(15, 2.4)	0.37	6.9			
149438	τ Sco	352	+13	B0V	2.82	-0.25	0.05	260	3.5	A	5	0.44	17.(15, 1.6) 19.(3, 1.6)	0.40	5.4	<0.60(4)		1.0(9)
149757	ζ Oph	6	+24	O9.5Vnn	2.57	+0.02	0.32	180	5.0	A	2	0.90	11.(1) 18.(3, 4.7) 14.(6) 16.(15, 2.3)	0.48	3.6	3.7(4) 2.6(12) 49.(18)	0.73(18)	1.3(9) 1.6(5) 8.8(2)
151890	μ^1 Sco	346	+4	B1.5IV	3.02	-0.23	0.02	220	3.5	B	7	0.51		0.11	4.8			
157056	θ Oph	0	+7	B2IV	3.27	-0.22	0.02	200	3.0	B	8	0.49		0.16	4.3			
157246	γ Ara	335	-11	B1Ib	3.33	-0.13	0.06	590	8.0	A	6, 7	0.44		0.68	10.			
158926	λ Sco	352	-2	B1.5IV	1.62	-0.18	0.07	100	0.7	B	7	0.23		0.03	2.2			
160578	κ Sco	351	-5	B1.5III	2.41	-0.20	0.05	180	1.5	B	7	0.27		0.11	3.9			
184915	κ Agl	32	-13	B0.5IIIn	4.95	0.00	0.28	580	8.0	B	5	0.45	12.(3, 0.5) 17.(15, 0.5)	0.72	9.5	4.0(14)	3.0(13)	4.0(2)
202904	υ Cyg	81	-10	B2Ve	4.42	-0.10	0.14	200	15.	A	8	2.4	16.(3, 1.3)	0.25	4.3	<0.82(4) 0.58(12)		
203064	68 Cyg	88	-4	O8n	4.98	-0.01	0.30	720	15.	A	3, 4	0.67		0.34	15.	10.(12)	4.6(13)	2.8(9) 2.4(5) 6.2(2)
205021	β Cep	108	+14	B1III	3.23	-0.21	0.05	320	1.0	B	7	0.10	21.(3, 5.3)	0.51	6.3			
214680	10 Lac	97	-17	O9V	4.88	-0.20	0.11	740	7.0	A	2	0.30	11.(3, 5.3)	0.87	8.9	≥3.3(4) ∿5.0(14) 3.0(12)	1.6(14)	1.3(9) -0.4(5) 1.0(6)
224572	σ Cas	116	-6	B1V	4.89	-0.08	0.18	390	3.0	A	7	0.25	16.(3, 5.1)	0.30	8.3	6.2(12)		

Table 1. References

(1) Goldstein and MacDonald (1969)	(10) Muller (1958)
(2) Duke (1951)	(11) Clark (1965)
(3) Takakubo and Van Woerden (1966)	(12) Merrill et al. (1937)
(4) Hobbs (1969, 1971)	(13) Spitzer et al. (1950)
(5) Stoeckly and Dressler (1964)	(14) Routly and Spitzer (1952)
(6) Habing (1968)	
(7) Menon (1958)	(15) McGee et al. (1966)
(8) Linblad (1966)	(16) Dunham (1941)
(9) Wampler (1966)	(17) Howard et al. (1963)
	(18) Herbig (1968)

*Measured from data of Carruthers (1969) by Savage and Code (1970).

†For those 21 cm surveys where the beam was not centered on the star, we have listed after the reference number the angular distance (in degrees) between the star position and radio position.

with other observables. References for the data on Na I, Ca II, 21-cm column densities, and 4430 Å central depths are listed at the end of the table. When more than one prototype star is listed in column 12 we have evaluated column densities by using both stars and then averaging the results. Such a procedure was necessary for certain intermediate spectral types.

c) Error Estimate

For each column density listed in Table 1 we have indicated the uncertainty by a letter classification system. Classification A implies the probable error is such that the true N_H may be 30% lower or 40% higher than the quoted value. Class B corresponds to -40% and +60%, while C is -50% and +100%. For example, the star ϕ^1 Ori (see Fig. 5 and Table 1) has an estimated error of class A and therefore has a column density of $10 \times 10^{20} + 4 \times 10^{20} - 3 \times 10^{20}$ atoms cm^{-2}. These error estimates are based on a consideration of the quality of each OAO spectrometer scan and the degree of confidence we have in the use of the prototype spectra to reduce a particular OAO star.

The varying degrees of uncertainty in the OAO column densities arise from several sources. In a number of cases the OAO line profiles are poorly determined because of a large and uncertain background correction. In these cases an estimate of possible errors has been made by allowing the background correction to vary over permissible limits and determining the corresponding hydrogen column density for each background se-

lected. A source of error common to all the OAO column densities is that of an incorrect allowance for line blending. Errors of this type can occur for a number of reasons. For example, the stellar features in the prototype stars may differ somewhat from the features in the OAO star being analyzed because of (1) a spectral type mismatch, (2) a luminosity class mismatch, (3) large differences in element abundances between the prototype star and OAO star, (4) other differences due to the peculiar nature of certain stars being studied, and (5) possible atmospheric O_2 absorption at 1206 Å in some of the prototype spectra. We estimate the O_2 feature to have an equivalent width no greater than 1 Å and hence this possible feature would be relatively unimportant compared with the much stronger Si III stellar absorption at the same wavelength. We have obtained information on how large errors of type (1) and (2) can be by using several prototype stars to analyze a single OAO star. Our general finding was that when the interstellar hydrogen column densities are large ($N_H > 2 \times 10^{20}$ atoms cm^{-2}) the errors due to spectral class or luminosity class mismatches are small (class A and B errors). This was the consequence of line blending being less important when the interstellar L_α line dominates the stellar lines. In contrast, when the interstellar hydrogen column densities are small ($N_H < 2 \times 10^{20}$ atoms cm^{-2}) the effects of line blending are more important and small mismatches between the OAO star and the prototype star produce larger errors (generally class B and C). For this reason the stars with small hydrogen column densities in Table 1 are usually of class C error while the stars with large column densities are usually of class A error except in those cases where the OAO profiles are poorly determined.

As we saw in Figure 1, for every star observed at L_α the OAO spectrum scanner obtains information on a number of strong ultraviolet stellar lines, and we can verify that the prototype star with the most similar ultraviolet spectrum has been selected. Since the Si III (1206.5 Å) feature is a major source of line blending with L_α in the OAO data, it is particularly instructive to study the relative strengths of the prominent Si III (1300 Å) and Si IV (1400 Å) multiplets. Differences in these two silicon features between the prototype and subject star provides a gauge of the importance of any of the four earlier mentioned dissimilarities in reducing the accuracy of our L_α absorption measurement. For example, in Figure 1 we can see that the stellar lines of Si III and Si IV in τ Sco (B0 V) and δ Sco (B0.5 IV) are of similar strength. This observation gives one confidence that the use of the rocket data on δ Sco as a prototype for the column density determination in τ Sco is valid. Through comparisons of this type we have noted that for stars of spectral type B0 to B2, the spectra of stars of luminosity class V, IV, III and II are quite similar,

while the supergiants have much stronger ultraviolet lines (Bless and Code 1970). We therefore feel we are justified in using, for example, the prototype star γ Ori (B2 III) to analyze other B2 stars of luminosity classes ranging from V through II. For the O type stars the differences among luminosity classes are larger. However, in the case of O9.5 stars we have prototypes for luminosity classes V, II and I.

The column densities reported in Table 1 should in most cases pertain to the interstellar medium. Jenkins (1970a) has considered the possibility that L_α emission from the star or its surroundings might significantly modify derived interstellar column densities. His conclusion was that such modifications are very unlikely. A more relevant problem for the data presented here is that of determining if photospheric absorption at L_α is contributing to the observed hydrogen column densities. As we indicated earlier, stars of spectral types later than B2 were excluded from this paper because in such stars the stellar L_α line is very strong. For all of the stars listed in Table 1, we have plotted N_H vs. spectral type and have found no overall tendency to obtain larger column densities in the cooler stars. It will be apparent from the material presented in § IVc on the gas to dust correlation that for B2 stars the stellar L_α line does not significantly modify the derived interstellar column densities. On the other hand, a reasonable fraction of the L_α absorption could be stellar when the measured N_H is as low as approximately 10^{20} atoms cm^{-2}; hence it is probably wiser to consider these lower values as upper limits for the interstellar N_H.

d) Comparison of OAO and Rocket Column Densities

A comparison of our results with various rocket column densities is given in Table 2. For the prototype stars we have listed the results obtained from measurements different from the ones we have employed for our comparisons. It is reassuring to note that the N_a values we have used do not differ appreciably from the values of the other investigators. In the case of the prototype star γ Ori, our determination of N_a from Carruthers' (1968) data is somewhat larger than his own measurement. The N_H values for the remaining stars in the right hand portion of the table were all derived from the OAO data by the technique discussed in § IIIb. For these stars roughly half show good agreement (γ Cas, ι Ori, α Vir, β^1 Sco, σ Sco and ω^1 Sco) while the rest disagree considerably with the OAO column densities. For η Ori and σ Ori the differences can be understood as due to the low quality of these particular rocket spectra. For β CMa the OAO value has a C error estimate, and in addition, Carruthers' spectrum for this star was of low quality (private communication). With κ Ori, ε Per

Table 2. Comparison of OAO and Rocket Column Densities

Prototype Stars

Star	Spectral Type	N_a 10^{20} cm^{-2}	N_H(rocket)	Reference
γ Ori	B2 III	0.65	$0.39^{+0.19}_{-0.15}$	3
δ Ori	O9.5 II-III	1.3	1.5	1
ζ Ori	O9.5 Ib	1.75	1.5	1
			$1.1^{+0.30}_{-0.26}$	3
			$1.1^{+0.5}_{-0.4}$	5
ζ Pup	O5 f	0.70	$0.59^{+0.17}_{-0.16}$	3
π Sco	B1 V, B2	6.3	$7.5^{+8.}_{-4.}$	6
δ Sco	B0.5 IV	12.5	$12.^{+6.}_{-3.}$	6
ζ Oph	O9.5 Vnn	5.0	4.2	10
			4.6 ± 1.5	

REFERENCES

1. Morton (1967)
2. Jenkins and Morton (1967)
3. Carruthers (1968)
4. Smith (1969)
5. Carruthers (1969)
6. Jenkins, Morton and Matilsky (1969)
7. Jenkins (1970b)
8. Carruthers (1970b)
9. Bohlin (1970)
10. Smith and Stecher (1971)

Table 2, continued

OAO Stars

Star	Spectral Type	N_H(OAO) 10^{20} cm $^{-2}$	OAO Error Estimate	N_H(rocket) 10^{20} cm $^{-2}$	Reference
γ Cas	B0.5 IVe	1.9	B	$1.0^{+1.1}_{-0.3}$	9
η Ori	B0.5 Vnn	6.0	A	$2.7^{+3.3}_{-2.0}$	2
θ Ori	O6p,O9.5 Vp	11.	B	$4.8^{+2.7}_{-2.1}$	5
σ Ori	O9.5 V	5.0	A	$2.7^{+1.5}_{-1.2}$	2
ι Ori	O9 III	1.5	B	$1.5^{+1.2}_{-0.8}$	2
				$0.67^{+0.3}_{-0.24}$	3
				$1.4^{+0.6}_{-0.4}$	5
κ Ori	B0.5 Ia	4.0	A	$0.89^{+0.33}_{-0.28}$	3
β CMa	B1 II-III	0.2	C	$0.57^{+0.48}_{-0.34}$	3
α Vir	B1 IV	0.4	B	<0.4	4
β^1Sco	B0.5 V	13.	A	$14.\pm6.$	7
σ Sco	B1 III	20.	A	$20.\pm3.$	7
ω^1Sco	B1 V	12.	A	$16.\pm4.$	7
ε Per	B0.5 III	3.0	B	1.1 ± 0.3	8
ξ Per	O7.5	20.	A	$4.2^{+1.9}_{-1.5}$	8

and ξ Per the column densities of Carruthers are all significantly lower than the OAO values. We believe the problem for these stars (and also his determination for γ Ori) could be related to that previously discussed by Savage and Code (1970) for θ^1 Ori C, for which it was shown that Carruthers (1969) had underestimated the equivalent width by placing a continuum level too low and by not allowing for the broad damping wings of L_α.

IV. DISCUSSION

a) The Distribution of Hydrogen

Of the 69 stars listed in Table 1, 81% are less than 500 pc away, and all but one are closer than 1 kpc. The proximity of observed stars is simply a manifestation of the magnitude limit for OAO observations of good quality at L_α. Over such a small distance scale, the observed distribution of interstellar atomic hydrogen provides relatively little insight on general features in the structure of our galaxy, such as spiral arms. Moreover, the well known grouping of O and B type stars into associations makes it inevitable that some limited sections of the sky are well sampled while other more extensive regions are left unobserved. In spite of these shortcomings, however, interesting conclusions on significant local excesses or deficiencies of gas from one region to the next may be drawn from the stars in our list. A strong suggestion of this variability came from earlier rocket observations (Jenkins, Morton and Matilsky 1969). We have here a large enough set of observations, all made by the same instrument, to over-rule any earlier misgivings one may have had that the differences in hydrogen densities were attributable to systematic errors arising from the markedly different wavelength resolutions of the separate rocket flights or the differences in spectral types of the stars available.

The information on distance r and average volume density n_H in Table 1 is plotted in Figure 6a in the form of ellipses whose centers are located at the galactic coordinates for the appropriate star. The length of an ellipse's horizontal axis is proportional to r and the vertical axis corresponds to n_H. It follows that the area of each ellipse is proportional to the measured column density N_H. One can immediately see from this plot that the hydrogen gas distribution is not at all uniform. Certain areas of the sky stand out as being characteristically rich or deficient in hydrogen.

In trying to assess the degree of variability in the L_α column density measures, it is helpful to compare the observations with what one would expect to obtain if the hydrogen were perfectly uniform except for a stratification parallel to the ga-

lactic plane. For the z dependence of the volume density n_H we shall adopt the distribution given by Schmidt (1957) scaled to a thickness between half-density points of 220 pc (Schmidt 1957, McGee and Milton 1964). The density is normalized to 0.71 atom cm^{-3} for z = 0, which corresponds to a compromise between the $N_H = 3.5 \times 10^{20}$ csc |b| atom cm^{-2} relation observed somewhat away from the galactic equator by McGee and Murray (1961) and the 2.5×10^{20} csc |b| atom cm^{-2} result of Goldstein and MacDonald (1969). The expected amount of hydrogen the model would give to each star is shown in column 16 of Table 1. The vertical axis of each ellipse in Figure 6b has a length proportional to the L_α N_H, whereas the horizontal axis corresponds to the expected density for the simple distribution. The shape of the ellipses depict excesses or deficiencies of gas, which is basically the same information given in Figures 4 and 5 of the article by McGee and Murray (1961).

With the exception of a few of the Orion stars, the observations indicate a general deficiency of gas in the 180-270° sector of galactic longitude (an average of n_H over all of the stars in this area is 0.27 atom cm^{-3}). Three stars on the order of 1 kpc away and near the galactic plane, 139 Tau, 15 Mon and UW CMa, have n_H equal to 0.24, 0.061 and 0.12 atom cm^{-3}, respectively. This suggests that the lack of hydrogen in this area of the sky may not be confined to only the local few hundred pc distance which is typical of most of the stars covered in our survey. A deficiency in 21-cm emission near ℓ = 240° may be seen in both the plots of integrated brightness temperature of McGee and Murray (1961) and the contours of peak brightness temperature shown by McGee, Murray and Milton (1963) (perhaps best seen in Figure 4 of the latter article). This 21-cm minimum does not appear to extend as far back in longitude as 15 Mon (ℓ = 203°) or 139 Tau (ℓ = 184°), however.

Some of the reduction in N_H for ζ Pup (ℓ = 256°, b = -5°) may be attributed to the ionization of hydrogen within the Gum Nebula which surrounds this star (Gum 1955, Rodgers et al. 1960). The only other line of sight we observed which intersects this nebula is that toward UW CMa (ℓ = 238°, b = -5°), but this star is very distant, and only the outer edge of the nebula is in the way, so the ionization would probably be of negligible importance. Brandt, Stecher, Crawford and Maran (1971) have suggested that ionization of the interstellar gas occurs well outside the apparent boundary of the nebula. They made use of the earlier measured low N_H to ζ Pup and γ Vel, together with an estimate of 0.4 atom cm^{-3} for n_H in the neighborhood of the sun, to argue that the volume of the ionization extended to within 60 pc of the sun. Such an interpretation would appear to be substantiated by our observation that neutral hydrogen seems to be deficient over a very wide angle in

Figure 6a.—Pictorial representation of the distribution of interstellar hydrogen observed by the OAO. In both plots the centers of the ellipses correspond to the galactic coordinates (System II) of the stars observed. In (a) the total length of the horizontal axis of each ellipse is proportional to the star's distance, and the vertical axis is equal to the average volume density of gas along the line of sight. The area of each ellipse therefore is proportional to the column density that was measured.

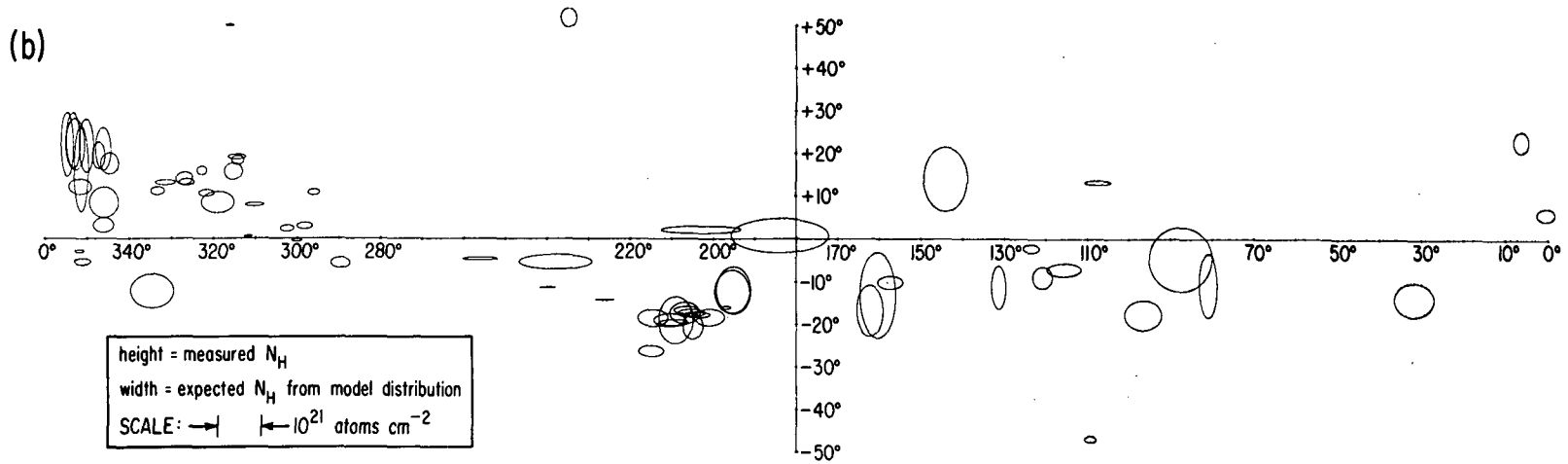

Figure 6b.—A comparison of the measured column density (vertical axis) for each star against what one would expect if the hydrogen were horizontally stratified according to Schmidt's (1957) $n_H(z)$ distribution normalized to 0.71 atoms cm^{-3} at $z = 0$. The dashed boundaries with identifying symbols define groups of stars which are distinguished from one another in the correlation plots (Figures 7, 8 and 9).

this region. On the other hand, it is hard to understand why the dispersion measures of MP 0818 (ℓ = 237°, b = +12°), PSR 0628-28 (ℓ = 237°, b = -17°) and CP 0834 (ℓ = 220°, b = +26°) are significantly less than PSR 0833-45, MP 0835 and MP 0736 located well inside the nebula (Gott and Ostriker 1971). It therefore seems more plausible that the ionization is still confined to the 40° diameter nebula, and that there is simply less interstellar gas in this particular area of the sky.

Another area which is prominent in Figure 6a is a small patch in Scorpius where the gas density is particularly rich. Although there is a spur of 21-cm emission projecting out of the galactic plane in this general neighborhood, details of the emission contours mapped in Figure 1(a) by McGee et al. (1963) do not correlate closely with the variations from one Scorpius star to the next. This might be an indication that these stars are embedded in a cloud complex, with some stars in front and others behind or within the gas cloud. (The properties of the medium in this region have been discussed by Herbig (1968) and Johnson (1970, 1971)).

It would be tempting to use the $L\alpha$ results to actually determine the general behavior of $n_H(z)$ in the solar vicinity since in each case an observation of $N_H \sin|b|$ is an average measure of $\int_0^{z(star)} n_H(z)\, dz$ along the line of sight. Unfortunately the plot of log $N_H \sin|b|$ vs. log z for our observations in Figure 7a shows considerable scatter, and it is difficult for us to define any systematic departures from the concept that n_H does not vary with z. (In this and succeeding figures in this paper, we have plotted the assigned A, B or C error code for each point instead of error bars to eliminate clutter.) Figure 7a, along with displays in Figure 6, helps to emphasize the strong irregularity in the H I gas distribution. We feel, however, that this type of display can be misleading because at high z we cannot avoid preferentially viewing toward isolated enrichments of gas projecting out of the galaxy, since it is precisely in such areas one usually finds young stars. If our sampling of directions were truly random (which it is not), the plot would be more meaningful. Similarly, we feel that any attempt to find some simple distribution which best fitted our data (such as the determination of the plane of the local gas layer in the manner of Goldstein and MacDonald (1969)) will be more a reflection of the irregularity of our sampling procedure, rather than a true generalization on the local distribution of hydrogen gas.

Figure 7a shows that 78% of the stars we observed have an average volume density n_H somewhere between 0.1 and 1.0 atoms cm^{-3} along the lines of sight. An average n_H for all of the stars equal to 0.6 atoms cm^{-3} was obtained over a mean dis-

tance of 300 pc from the sun. The average color excess per unit distance Σ E(B-V)/Σ r for these stars is equal to 0.31 mag kpc^{-1}. On the other hand, an average figure for the general reddening within 1 kpc of the sun is 0.61 mag kpc^{-1} (Spitzer 1968), which is roughly twice our average for the OAO stars. This difference demonstrates that our magnitude limit $V \gtrsim 5$ for L_α scans imposes a bias against the more heavily obscured stars at large distances. Hence, if one were to assume that the ratio of hydrogen to dust is constant everywhere (see § IVc and Fig. 9), a representative figure for the density over all directions would be twice the average n_H we have derived. There are seven stars closer than 140 pc for which the average n_H is 0.25 atoms cm^{-3}. We do not expect these nearby stars to be subject to the aforementioned observational selection.

Figure 6a or 6b reveals that of all the stars observed, a considerable fraction share some characteristic with their neighbors. We have already singled out for discussion the hydrogen-rich Scorpius region and a collection of stars having anomalously low column densities. The stars in Orion are all located within a reasonably confined solid angle, and stars in Crux, Centaurus and Lupus ($\diamond$), although fairly spread out, all have nearly the same distance modulus. It is of benefit to later discussions on the correlations of N_H with other observables to define memberships in groupings, even though the assignments are somewhat arbitrary. We have designated four groups, shown by the dashed perimeters in Figure 6a, and have put the remaining stars into a classification of "other" since they seem to be reasonably heterogeneous with respect to N_H, r and position in the sky. The symbols accompanying the regions in Figure 6a identify the membership of each star in the correlation plots (Figures 7, 8 and 9) and column 11 of Table 1.

In the introduction (§ I) we mentioned that the findings of the sounding rocket observers generally indicated the local hydrogen density was lower than previously suggested by overall surveys of 21-cm emission. More specifically, flights by several investigators clearly demonstrated that only occasionally did one find a L_α measurement yielding a column density as high as that suggested by the 21-cm emission in the same direction. This would not have been surprising for low galactic latitude stars since much of the 21-cm emission would have originated from portions of the galaxy beyond the stars, but a number of stars with $|b| \gtrsim 10°$ exhibited densities a factor of 10 lower than the corresponding 21-cm measures (Jenkins 1970a).

We are now in a position to repeat the comparison with the 21-cm data on a much wider scale. Figure 7b is a logarithmic plot of the L_α N_H against the 21-cm measures listed in column 14 of Table 1 for stars with $|b| > 10°$. For some of the stars we have observed, we could draw upon the results reported by

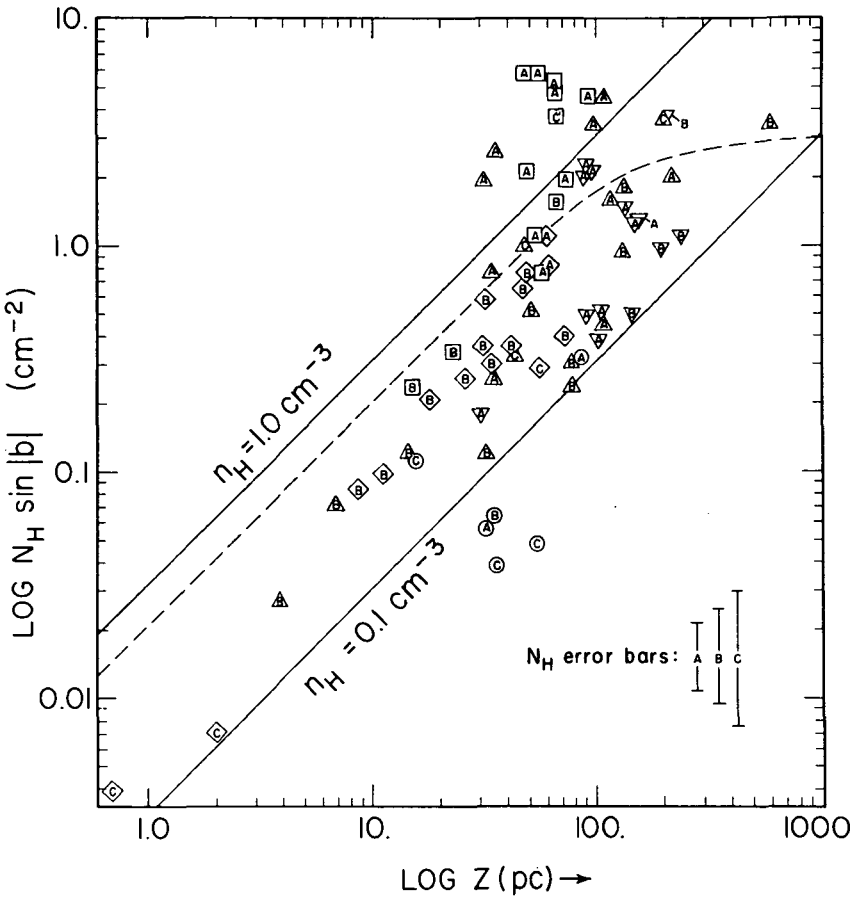

Figure 7a.—N_H sin |b| values plotted are an average measure along the line-of-sight of the amount of hydrogen situated between the z distance of a star and the plane of the galaxy (i.e., $N_H \sin |b| = \int_0^{z(star)} n_H(z)\,dz$ if n_H depends only upon z). The dashed line shows the expected behavior of the measurements if $n_H(0) = 0.71$ atoms cm^{-3} with a decrease in density away from the galactic plane following the distribution given by Schmidt (1957).

Habing (1968), Goldstein and MacDonald (1969) or Hobbs (1971), where the 21-cm emission has been sampled from a small diameter (1/2°) beam centered on the star's position (for the express purpose of comparing 21-cm and visual absorption line data). For many other cases, however, we had to rely on a measurement taken on the nearest grid point in the routine surveys of the other investigators referenced in the table. In each case we have shown in the tabulation the distance of the

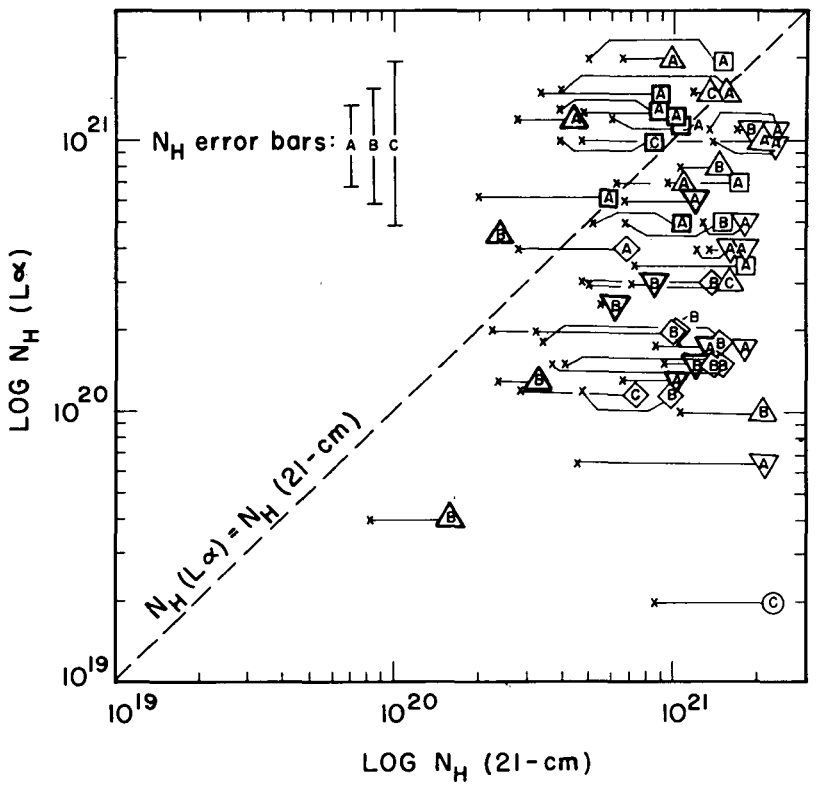

Figure 7b.—A correlation of L_α N_H measurements (at $b > 10°$) against 21-cm emission measurements (see column 14 in Table 1) in the same direction. The lines away from the left of each symbol indicate an estimated downward correction of the 21-cm results to compensate for background emission beyond the stars (see § IVa). The shapes of the plotted points show the star locations as defined in Fig. 6a, and the bolder symbols indicate the small-beam observations directly centered on the stars.

survey point from the star. We expect to have the closest correspondence with the centered observations; for Figure 7b we have chosen these measurements, when available, in preference to the survey values and plotted the symbols more boldly to emphasize their greater relevance to our measurements. For the surveys by Takakubo and van Woerden (1966) and Linblad (1966) we added up the N_H values given for the Gaussian components of optical depth, which were computed under the assumption that the spin temperature equalled 125°K. For all of the other references, we listed N_H simply computed from the integral of brightness temperature over frequency, which invokes the assumption that $\tau_{21\text{-cm}} \ll 1$. The fact that optical depths often

are not negligible means that the column densities computed by the latter method are usually somewhat lower than the true values.

Figure 7b demonstrates that the OAO data show virtually no correlation with the 21-cm emission measurement. A large majority of the column densities deduced from the 21-cm data are higher than those obtained from the L_α absorption measurements. To some degree, one would generally expect to find higher N_H values from the 21-cm data because of the additional contribution from hydrogen beyond the stars we have observed. To obtain a rough estimate of how much the 21-cm N_H should be revised downwards to correct for the background emission, we may resort to the idealized model for $n_H(z)$ discussed earlier and say it is reasonable to multiply each 21-cm result by the factor

$$x = \frac{\int_0^{z(\text{star})} n_H(z)\,dz}{\int_0^{\infty} n_H(z)\,dz} \qquad (2)$$

where the integral to infinity equals 3.0×10^{20} csc $|b|$ atoms cm^{-2}. The factor x is tabulated for each star in column 15 of Table 1, and each point plotted in Figure 7b has a line extending toward the left (ending at an "x") whose length corresponds to the logarithm of the correction factor. Even with the x corrections, however, most of the points still lie well below the diagonal $N_H(L_\alpha) = N_H(21\text{-cm})$ line. For stars above this line, it is likely that saturation of the radio emission is causing us to underestimate the 21-cm N_H.

b) Correlation of H I with Na I and Ca II

Measures of the interstellar D line absorption of Na I and the H and K lines of Ca II have been made for many of the stars in our program, as is evident from the many entries in columns 17 and 18 of Table 1. A comparison of H I to Na I and Ca II column densities should allow us to derive reasonably secure values for the overall abundance ratios in the interstellar medium, as well as to carry out a limited study on how much these ratios fluctuate over the various lines of sight. Past studies of this nature (Lawrence 1956, Howard, Wentzel and McGee 1963, Takakubo 1967, Habing 1968, Habing 1969, Goldstein and MacDonald 1969, Hobbs 1971) have had to contend with the uncertainty of how well the optical column corresponded with the 21-cm beam. We have seen from the results of the previous section that even for small radio beams exactly centered on a star, the 21-cm measurement is not very representative of the column density to the star. The earlier investi-

gators, however, did have the opportunity to use the velocity information in both the 21-cm emission and visible absorption data to help resolve this problem. Interesting conclusions from the earlier investigations on the correlations of specific velocity components cannot, of course, be verified or explored further with the L_α results.

The equivalent widths of both components of the doublets have been obtained by the investigators referenced in the appropriate columns of Table 1, with the exception of Hobbs (1969), who observed with an interferometric, photoelectric scanner and displayed high resolution (0.5 km sec^{-1}) tracings of the D2 line (and also the D1 line when D2 appeared to be saturated). For all but Hobbs' data, we have made use of Strömgren's (1948) Table 2 to derive column densities by the doublet ratio method, except for a revision of the transition f values to those given by Wiese, Smith and Miles (1969) of 0.327 for D1 and 0.344 for H. For the cases where the doublet ratio exceeded 2.0, we used the procedure of Routly and Spitzer (1952) of equating W_{D1} to $(W_{D1} + W_{D2})/3$ and assuming the lines were completely unsaturated. Occasionally, only an upper limit for the equivalent width of one component was available for a particular star. In this situation we derived column density upper limits assuming the line was weak enough that no saturation occurred. The two entries for Ca II in β^1 Sco (HD 144217) exemplify that this assumption may not always be valid and that such upper limits are not entirely trustworthy.

The greater profile accuracy and detail in the sodium data of Hobbs (1969) warrant a treatment which does not rely upon the simplifying assumption on the velocity behavior which is inherent with the doublet ratio method. As long as the residual intensity at the line center is not near zero, we can derive the neutral sodium column density from a straightforward integration of the measured optical depth over frequency,

$$N_{Na\ I} = \frac{mc}{\pi e^2 f_{12}} \int \tau d\nu = \left\{ \begin{matrix} 1.96 \times 10^{11} (D1) \\ 9.8 \times 10^{10} (D2) \end{matrix} \right\} (km\ sec^{-1})^{-1}\ cm^{-2} \int \tau dv \qquad (3)$$

Optical depths τ greater than 3.0 were hard to measure accurately and 4.6 was the maximum value we could include in the reduction. For stars having an absorption much stronger than $\tau = 3$ over a significant fraction of the profile's total velocity spread, the measurements very likely underestimate the true column densities, and hence these values were quoted as lower limits in Table 1. When available, D1 line values were listed in preference to the more saturated D2 line determinations. For some stars, we noticed that a large fraction of the τ_{D2} measurements ranged from 10 to 40% lower than the ex-

pected value of $2\tau_{D1}$ at the same velocity. This effect occurred for τ_{D2} significantly less than 3, and we conclude this may be an indication that for some cases the 0.5 km sec^{-1} resolution was not quite adequate for resolving saturated fine structure in the profiles. Hence it is possible that even some of the determinations not having excessive τ values may slightly underestimate the true Na I column density.

Occasionally, telluric water vapor absorptions appeared along with the D2 profiles. Hobbs pointed out this contamination when it occurred in his data, and in such situations we either totally relied upon the D1 profile (if available) or we eliminated the water peaks from the integration if they were small and separable. At times we could make use of only D2 tracings which had strong water lines blended with the sodium absorption, and in such cases we quoted the Na I column density values as upper limits in Table 1 and Figure 8a without attempting to separate out the spurious absorption since we could not estimate its strength. Stars having both large sodium optical depths and water vapor lines have values designated as approximate ($\sim$) in the table.

When the Na I column density has reached a value well in excess of that necessary to saturate the D lines, the 3302 doublet becomes strong enough to measure. Once again the ratio method can be used to derive a figure for $N_{Na\ I}$ by now comparing the 3302 and D line strengths (Strömgren 1948). Herbig (1968) used this approach to arrive at $N_{Na\ I} = 4.9 \times 10^{13}$ atoms cm^{-2} to ζ Oph (HD 149757). As noted by Herbig (1968) and Hobbs (1971), the doublet ratio method applied to the D lines fails for such large column densities, and it appears that even our value of 3.7×10^{12} atoms cm^{-2} derived from integration of the high resolution data is far lower than Herbig's result. The discrepancy with our method is rather puzzling in view of the fact that Herbig's curve of growth shows the optical depth $\tau_0 = 56$ for the center of the D1 line, whereas the largest τ seen in the D1 tracing of Hobbs (1969) is about 2.4. The residual intensity measured at the bottom of the strong D1 profile seems, by a good margin, to be larger than either the statistical noise or any reasonable uncertainties in subtracting off the parasitic light and dark current contributions described by Hobbs, although the profile does appear to have a slightly flattened bottom which suggests saturation.

In view of the aforementioned disagreement, we are somewhat skeptical of the larger $N_{Na\ I}$ values quoted in Table 1. In deriving a representative average value for the density ratio $\langle Na\ I/H\ I \rangle$ we disfavored the larger $N_{Na\ I}$ measurements as well as those where only upper limits were available. Estimates of 3.5×10^{-9} for $\langle Na\ I/H\ I \rangle$ and 2.5×10^{-9} for $\langle Ca\ II/H\ I \rangle$ were derived from a visual inspection of Figures 8a and 8b, where points in the middle of the sequences were

given the greatest weight. Our value for $\langle$Na I/H I$\rangle$ is in excellent agreement with an average given by Hobbs (1971) of 4×10^{-9}.

A large fraction of the interstellar sodium and calcium atoms are expected to be in the ionization state just higher than that observed, since both Na I and Ca II can be ionized by starlight photons less energetic than the Lyman limit at 13.6 eV. Hence, to deduce representative values for the total element abundance ratios $\langle$Na/H$\rangle$ and $\langle$Ca/H$\rangle$, one must evaluate the equations for ionization equilibrium and accordingly apply large corrections to the observations of Na I and Ca II. In the case of sodium, for any point along the line of sight we may consider the balance of photoionization of Na I against recombinations of free electrons and Na II,

$$\Gamma n_{\text{Na I}} = \alpha n_{\text{Na II}} n_e \quad , \tag{4}$$

and assume all of the sodium has a fixed abundance relative to hydrogen and exists only in neutral or singly ionized form,

$$n_{\text{Na}} = n_{\text{Na I}} + n_{\text{Na II}} = (n_e + n_{\text{H I}}) \langle \text{Na/H} \rangle \tag{5}$$

to arrive at the relation

$$\langle \text{Na/H} \rangle = n_{\text{Na I}} \frac{1 + (\Gamma/\alpha n_e)}{n_{\text{H I}} + n_e} \quad . \tag{6}$$

The above equation may also be recognized for the relation of $\langle$Ca/H$\rangle$ with respect to $n_{\text{Ca II}}$. The accuracy of the ionization calculations, however, is severely limited by our incomplete knowledge about conditions along any path through the interstellar medium, as well as some uncertainties in the ionization and recombination cross sections. Nevertheless it is instructive to evaluate an estimate for total element abundances based on reasonable estimates for the relevant parameters, even if many of the choices seem to be rather arbitrary and hypothetical.

A recent survey by Radhakrishnan, Murray, Lockhart and Whittle (1971) of 21-cm emission and absorption in the direction of 35 extragalactic sources suggests that the hydrogen is about equally divided between cool, dense clouds and a surrounding hotter medium. These observations, together with an interpretation by Hjellming, Gordon and Gordon (1969) on conditions in the direction of three pulsars, suggest that we could adopt the picture that, on the average, about 5% of any line of sight has roughly 5 H atoms cm^{-3} at 60°K and the remaining 95% contains 0.26 atoms cm^{-3} of hydrogen at 1000°K. Pressure balance is maintained in this model, and the overall

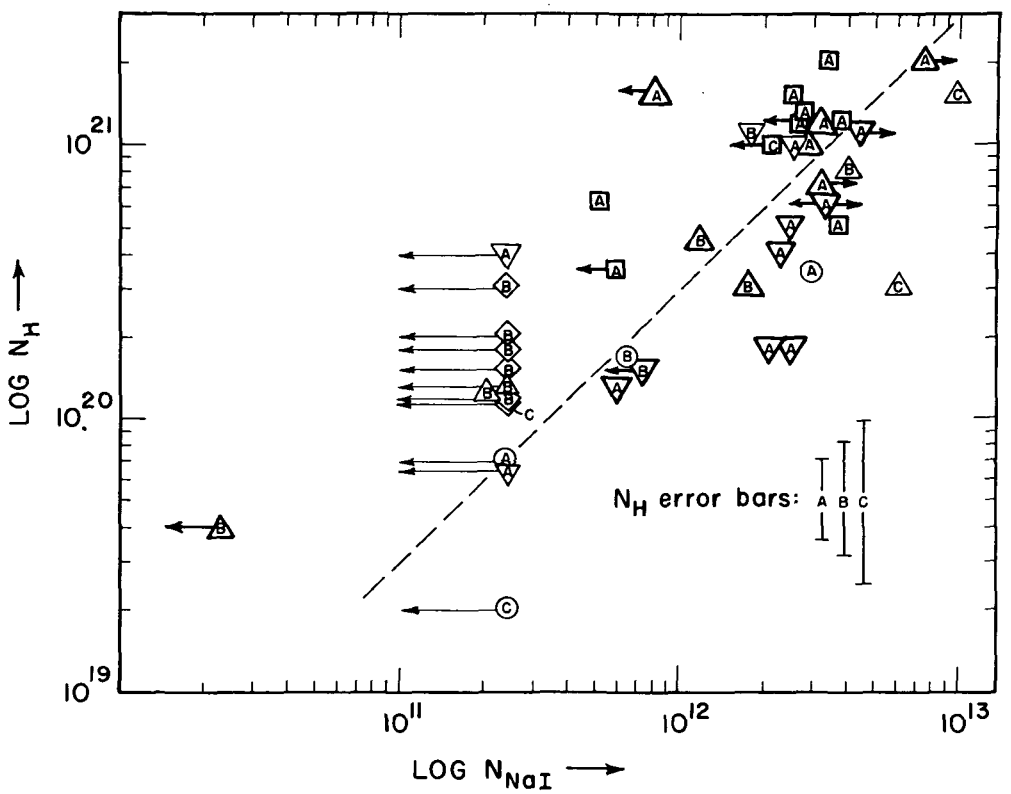

Figure 8a.—Correlation plots of the N_H measurements for those stars where we could obtain Na I and Ca II column densities (or their upper limits) by applying the doublet ratio method to equivalent width measurements or by integrating the D line optical depths over velocity in the high resolution observations of Hobbs (1969). The latter method of obtaining $N_{Na\ I}$ is considered more reliable than the former, and these better values are plotted with symbols having a bold border. The dashed lines correspond to our estimate for the average ratios of Na I and Ca II to H I of 3.5×10^{-9} and 2.5×10^{-9}, respectively.

n_H corresponds to 0.5 atoms cm^{-3}, which is a good representative value for the more trustworthy measures of Na I, Ca II and H I column densities. For electrons produced from ionizations of H I by X-rays or low energy cosmic rays, we expect to find

$$n_e \alpha n_H^{0.5} T^{0.35} \qquad (7)$$

if the ionization rate is constant everywhere (Habing 1969). Densities of 0.042 and 0.026 electrons cm^{-3} for the cold and

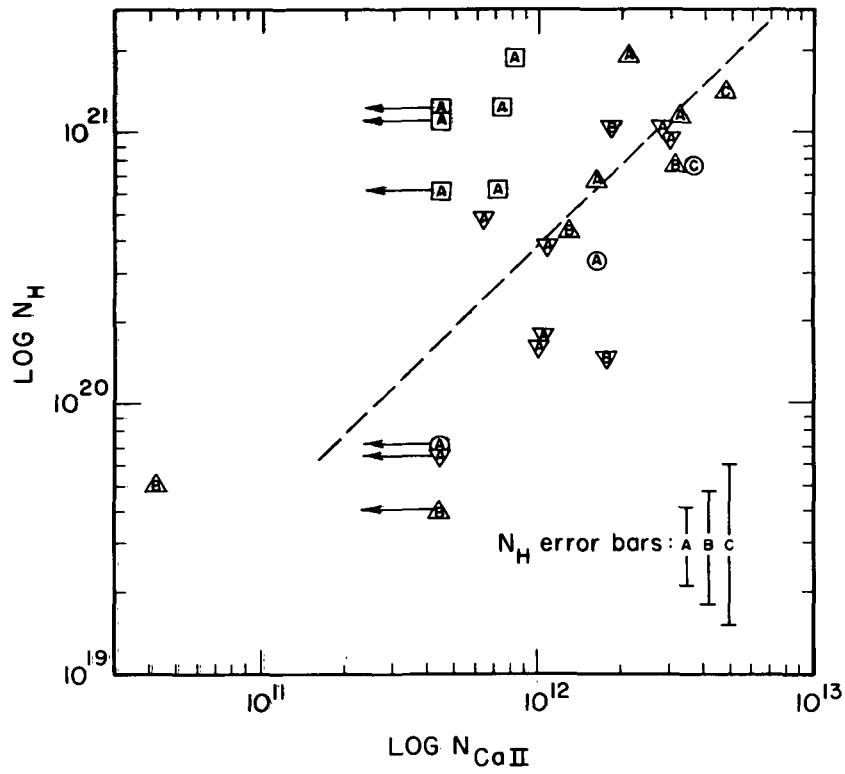

Figure 8b.—See Figure 8a caption.

hot portions, respectively, are consistent with equation (7) and the observed average of 0.03 electrons cm^{-3} for dispersion measures of pulsars at known distances (Davidson and Terzian 1969, Lang 1971). Our interpretation of the dispersion measure integral includes an extra rms fluctuation term (Lerche 1970) whose value corresponds to the expected variations of n_e between the two regions. Habing (1969) estimates representative values for Γ/α in the interstellar medium equal to $2.1(T/100)^{0.7}$ for Na I and $0.04(T/100)^{0.7}$ for Ca II. Substituting these values into equation (6) we find $\langle Na/H \rangle = 2.3 \times 10^{-7}$ and $\langle Ca/H \rangle = 6.8 \times 10^{-9}$ is consistent with both the model and our averages for the observed $\langle$ Na I/H I $\rangle$ and $\langle$ Ca II/H I $\rangle$ quoted earlier. These element abundance ratios are a factor of 7 and 230 below the cosmic abundance of 1.6×10^{-6} for both $\langle Na/H \rangle$ and $\langle Ca/H \rangle$ (Allen 1963). If we instead adopt a model for the interstellar medium closer to that suggested by Field, Goldsmith and Habing (1969) (3% of the volume with $n_H = 30$ atoms cm^{-3} and $T = 60°K$ surrounded by $n_H = 0.1$ atom cm^{-3} at $10^4°K$) and apply the same analysis as before, we obtain the even lower values of $\langle Na/H \rangle = 1.0 \times 10^{-7}$ and

$\langle Ca/H \rangle = 4.0 \times 10^{-9}$.

Figures 8a and 8b show the observed $N_{Na\ I}/N_H$ and $N_{Ca\ II}/N_H$ ratios are generally lower for the Scorpius stars (□) than for most of the others. This relative deficiency has been noted earlier for these stars by Buscombe and Kennedy (1968) in their comparisons of the interstellar lines with color excesses. We previously suggested (in § IVa) that large N_H values measured for the Scorpius region may result from a relatively dense gas complex near these particular stars. We can surmise from Figure 7b that much of this gas is probably rather cool since, as an exception to the rule, the $L\alpha$ N_H measurements are greater than the indications from 21-cm emission (i.e., $\tau_{21\text{-cm}} > 1$ and thus $T \gtrsim$ peak $T_b \approx 50°K$). If we combine equations (6) and (7) with the $T^{0.7}$ dependence for Γ/α, we would expect the extra gas near the Scorpius stars, which is probably cooler and denser than average, to exhibit larger $\langle$ Na I/H I $\rangle$ and $\langle$ Ca II/H I $\rangle$ ratios than usual—just the opposite to what is observed. It is possible, on the other hand, that the proximity of the stars to the gas may raise the ionizing radiation flux significantly above what is usually found in the galaxy.

c) Correlation of H I with Dust

A number of previous investigations have dealt with the relationship between interstellar hydrogen and interstellar dust. For a review of these observations see Kerr (1968). All these studies have utilized 21-cm emission or absorption data along with a number of different techniques to obtain line-of-sight extinction. However, our poor correlation of 21-cm and $L\alpha$ column densities exposes the weakness of the assumption that the 21-cm radio observations of the gas and the optical observations toward stars refer to the same regions of space. With the OAO $L\alpha$ absorption data and optical extinction data, one samples precisely the same regions of space so it is now possible to make a more reliable study of the H I to dust correlation.

Figure 9 shows the relationship between the OAO hydrogen column density and the E(B-V) color excess for all the stars included in Table 1. Lower case error symbols refer to B2 stars while capital letters refer to stars of spectral type earlier than B2. The subscript é on a symbol indicates an emission line star for which the computed E(B-V) color excess is probably affected by the emission.

In Figure 9 one can see a strong correlation between the hydrogen column density and color excess. The B2 stars do not lie significantly above the earlier type stars, which indicates that for B2 stars it is reasonable to assume that the stellar $L\alpha$ line is contained within the core of the interstellar line

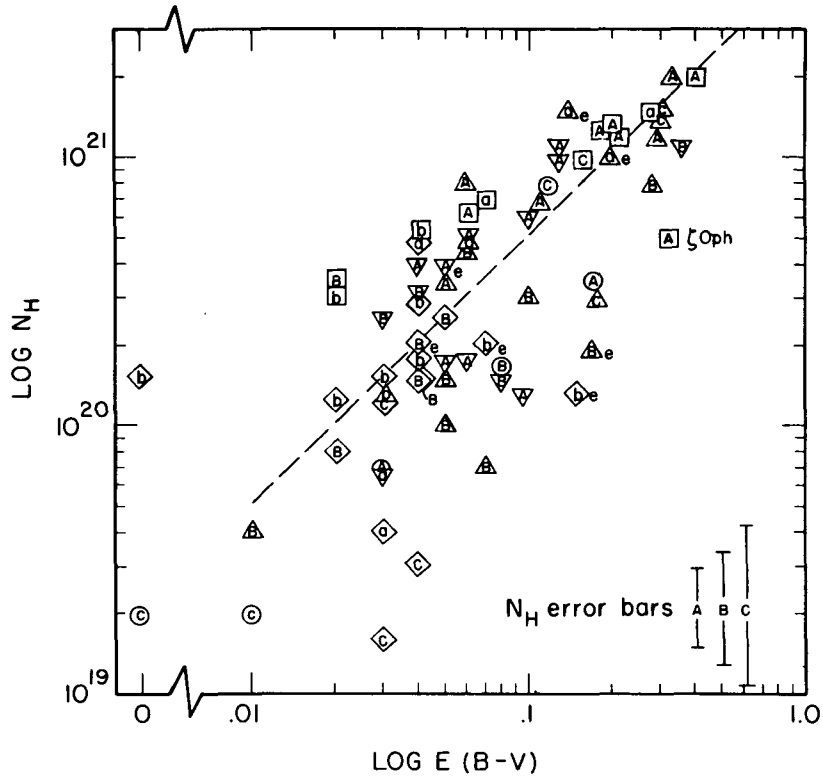

Figure 9.—A comparison of measured N_H versus B-V color excess for all of the stars observed. Symbols followed by an e are classified as emission line stars; we expect their E(B-V) values to be somewhat unreliable. Lower case error symbols identify the B2 stars. The dashed line represents our weighted average of 5×10^{21} atoms cm^{-2} mag^{-1} for the observed H I to E(B-V) ratios.

for most of the objects considered here. We found the situation to be quite different for stars of spectral type B2.5 or later. For these stars, it was apparent from the line strengths in unreddened objects that stellar $L\alpha$ was very strong. Because of these considerations we omitted all stars of spectral types later than B2 from this paper.

The points in Figure 9 show a fair amount of scatter. Some of this is definitely observational while some is definitely real. For example, several Be stars deviate significantly from the general correlation. In the figure the scatter is largest for stars with small color excesses. Much of this scatter can be understood as small errors ($0^m.02$) in the color excess determinations. In addition, the OAO column density measurements are less accurate for stars with small column densities due to the greater effect uncertainties in line blending

have on the L_α profiles.

The data plotted in Figure 9 can be used to estimate the mass density ratio of H I to dust in the interstellar medium. Previous estimates from the radio data are summarized by Kerr (1968). A mean of the numbers from various determinations (Kerr's Table 4) is $\langle \rho_{H\ I}/\rho_{dust} \rangle \approx 100$, although the determinations vary from a low of 8 to a high of 300. Using the OAO L_α data for stars other than Be stars and weighting each determination by the color excess we obtain,

$$\langle N_H/E(B-V) \rangle = 5 \times 10^{21} \text{ atoms cm}^{-2} \text{ mag}^{-1} \quad . \quad (8)$$

To relate H I and dust densities it is necessary to assume a grain model. The radio investigations mentioned above generally assumed a model consisting of a grain radius $A_g = 3 \times 10^{-5}$ cm, a grain density $\rho_g = 1$ gm cm^{-3}, and an extinction efficiency factor $Q = 2.0$. With this very simple model plus the assumption that the ratio of selective to total visual extinction $R_V = 3.0$, one can find from the relations given by Lilley (1955) and equation (8) that the OAO data imply $\langle \rho_{H\ I}/\rho_{dust} \rangle \approx 50$.

However, it is possible to obtain an improved estimate by using the best interstellar grain model presently available. The theoretical mixture of grains of graphite, silicon carbide and silicates of Gilra (1971) has been shown to reproduce reasonably well the basic observational data (including ultraviolet extinction) on interstellar grains. Gilra (1971) finds on the basis of his mixture of grains that a space density of 8×10^{-27} gm cm^{-3} is needed to produce 1 mag kpc^{-1} of extinction at the V filter. Again assuming $R_V = 3.0$ we find from equation (8) that this mixture implies $\langle \rho_{H\ I}/\rho_{dust} \rangle \approx 100$.

The general appearance of the distribution of points in Figure 9 suggests the existence of a relatively well-defined edge parallel to and above the dashed line which corresponds to the mean $N_H/E(B-V)$. On the other hand, there is a significant straggling of the points below the line. We could speculate that the upper edge (~2.5 times the number given in Equation 8) corresponds to an intrinsic total hydrogen to dust ratio, and that lower points in the diagram show evidence of varying degrees of depletion of atomic hydrogen by either molecule formation or ionization. One outstanding example of possible depletion is ζ Oph which is deficient of atomic hydrogen by about a factor of 3 from the average ratio we derived. The visual interstellar spectrum of ζ Oph is rich with molecular lines (Herbig 1968), and it is possible molecular hydrogen may also be abundant. McGee et al. (1963) observed a deficiency of 21-cm emission near ζ Oph which coincides with the Strömgren sphere for this O9.5 V star, but representative models for the size and density of the ionized re-

gion suggested by McGee et al. and Herbig imply the depletion of the observed N_H by ionization is negligible.

Carruthers (1970b) has observed a molecular hydrogen column density of 1.3×10^{20} molecules cm^{-2} in the direction of ξ Per. The fractional abundance by weight of molecular compared to atomic hydrogen implied by this number is about 0.13 if one uses the OAO hydrogen column density for ξ Per of 20×10^{20} atoms cm^{-2}. With such a low fractional abundance one might expect the $N_H/E(B-V)$ relation for ξ Per to be normal, and it is. An H_2 column density in the direction of ζ Oph of 5×10^{20} molecules cm^{-2} would explain the factor of 3 deficiency of H I. The implied difference in the H_2 abundance between these two stars might be explained by the fact that the far ultraviolet extinction in the direction of ζ Oph is much greater than for ξ Per (Bless and Savage 1972), and it is the far ultraviolet radiation field between 912 Å and 1108 Å that likely provides the destruction mechanism for the H_2 molecule (see Hollenbach et al. (1971) for a discussion on the formation and destruction of H_2).

V. CONCLUDING REMARKS

The primary data of our study are the hydrogen column densities toward the 69 stars listed in Table 1. The abstract summarizes a number of conclusions derived from a comparison of these column densities and other observables. We will not repeat these conclusions here but will indicate some additional projects that could be undertaken.

The comparison between 21-cm and L_α column densities discussed in § IVa would be more meaningful if one considered only the 21-cm observations with a small beam centered on each star and attempted to extract velocity components not appearing in the visual interstellar line data. For this project more star-centered radio observations are desirable.

In estimating the total sodium and calcium abundance ratios, it should soon become possible to reduce some of the uncertainties. The sky background ultraviolet flux used by Habing (1969) to estimate Γ can hopefully be replaced by OAO-2 broad-band photometry observations of this radiation field. Also, according to Hobbs (private communication), high resolution observations of the K line of Ca II should soon be available and will provide a more reliable Ca abundance estimate.

Column 19 of Table 1 contains data from Duke (1951), Stoeckly and Dressler (1964) and Wampler (1966) on the diffuse feature at 4430 Å. It should now be possible to investigate if this feature is more closely correlated with the interstellar gas or the interstellar dust. C. C. Wu (private communication) has undertaken an investigation of diffuse and semi-diffuse features in stars observed by the OAO. He has obtained

new observational data on the semi-diffuse features at 5780 Å and 5796 Å and will investigate the relationship between the central depths of 4430, 5780 and 5796 Å versus the L_α N_H, E(B-V) and E(2200 Å-V). In view of the work of Wu, we did not investigate the various correlations of diffuse features in this paper.

There remain a number of additional stars B2 or earlier for which L_α measurements can be made by OAO-2. We will try to observe these stars and fill some of the vacant areas in our sky coverage. Finally, as more high resolution prototype spectra become available, it should become possible to derive more accurate column densities for those OAO stars having large uncertainties. A rocket recently launched by the Kitt Peak National Observatory for the Princeton group obtained spectra for τ Sco (B0 V), κ Sco (B1.5 III) and λ Sco (B1.5 IV). Not only are these observations of excellent quality, but the actual column densities for the stars are relatively small so that reconstructions for small trial column densities will be more reliable.

Support for the preparation of this paper was provided by contracts NAS 5-1348 (for BDS) and NSr-31-001-901 (for EBJ) from the U. S. National Aeronautics and Space Administration. We wish to thank Dr. A. D. Code for making the OAO data available to us, and we are indebted to Drs. T. Houck, R. C. Bless, C. F. Lillie, A. Holm and M. Molnar for obtaining the observational material. Important contributions were made by C. C. Wu, who helped reduce the raw OAO data to derive useful L_α profiles, and J. Pritchard, who computed Na I column densities from the observations of Hobbs (1969). We are thankful to L. M. Hobbs for his helpful comments and advice about his high resolution measurements. Dr. G. R. Carruthers kindly provided us with an original tracing of his γ Ori spectrum. The Princeton rocket spectra were obtained on NASA flights 4.176UG, 4.226UG, and 4.271UG and were digitized by the microdensitometer at the Sacramento Peak Observatory. Finally, we wish to thank Mr. T. Matilsky for his help in deriving the intensity profiles of δ and π Sco and ζ Oph.

REFERENCES

Allen, C. W. 1963, Astrophysical Quantities, 2nd ed. (London: Athlone Press), p. 31.

Blaauw, A. 1963, Basic Astronomical Data, ed. K. Aa. Strand (Chicago: University of Chicago Press), p. 383.

Bless, R. C. and Savage, B. D. 1970, in Ultraviolet Stellar Spectra and Related Ground-Based Observations, I.A.U. Symp. No. 36, ed. L. Houziaux and H. E. Butler (Dordrecht: D. Reidel Publ. Co.), p. 28.

_____ 1972, preprint.

Bohlin, R. C. 1970, Ap. J. 162, 571.

Brandt, J. C., Stecher, T. P., Crawford, D. L. and Maran, S. P. 1971, Ap. J. 163, L99.

Buscombe, W. and Kennedy, P. M. 1968, M. N. R. A. S. 139, 417.

Carruthers, G. R. 1968, Ap. J. 151, 269.

_____ 1969, Ap. J. 156 L97.

_____ 1970a, Space Sci. Rev. 10, 459.

_____ 1970b, Ap. J. 161, L81.

Clark, B. G. 1965, Ap. J. 142, 1398.

Code, A. D. 1960, A. J. 65, 278.

Code, A. D., Houck, T. E., McNall, J. F., Bless, R. C. and Lillie, C. F. 1970, Ap. J. 161, 377.

Cousins, A. W. J. and Stoy, R. H. 1963, Bull. Roy. Obs. No. 64.

Davidson, K. and Terzian, Y. 1969, A. J. 74, 849.

Duke, D. 1951, Ap. J. 113, 100.

Dunham, T., Jr. 1941, Pub. A. A. S. 10, 50.

Field, G. B., Goldsmith, D. W. and Habing, H. J. 1969, Ap. J. 155, L149.

Gilra, D. P. 1971, Nature 229, 237.

Goldstein, S. J. and MacDonald, D. D. 1969, Ap. J. 157, 1101.

Gott, J. R., III and Ostriker, J. P. 1971, to appear in The Gum Nebula and Related Problems, ed. S. P. Maran, J. C. Brandt and T. P. Stecher, NASA.

Gum, C. S. 1955, Mem. R. A. S. 67, 155.

Habing, H. J. 1968, Bull. Ast. Inst. Netherlands 20, 120.

_____ 1969, Bull. Ast. Inst. Netherlands 20, 177.

Herbig, G. H. 1968, Z. Astrophysik 68, 243.

Hiltner, W. A., Garrison, R. F. and Schild, R. E. 1969, Ap. J. 157, 313.

Hjellming, R. M., Gordon, C. P. and Gordon, K. J. 1969, Astron. and Astrophys. 2, 202.

Hobbs, L. M. 1969, Ap. J. 157, 135.

_____ 1971, Ap. J. 166, 333.

Hollenbach, D. J., Werner, M. W., Salpeter, E. E. 1971, Ap. J. 163, 165.

Howard, W. E., Wentzel, D. G. and McGee, R. X. 1963, Ap. J. 138, 988.

Iriarte, B., Johnson, H. L., Mitchell, R. I. and Wisniewski, W. K. 1965, Sky and Telescope 20, 21.
Jenkins, E. B. 1970a, in Ultraviolet Stellar Spectra and Related Ground-Based Observations, I.A.U. Symp. No. 36, ed. L. Houziaux and H. E. Butler (Dordrecht: D. Reidel Publ. Co.), p. 281.
_____ 1970b, Presentation at Commission 44, I.A.U. 14th General Assembly (Brighton, England) August, 1970.
_____ 1971, Ap. J. 169, in press.
Jenkins, E. B. and Morton, D. C. 1967, Nature 215, 1257.
Jenkins, E. B., Morton, D. C. and Matilsky, T. A. 1969, Ap. J. 158, 473.
Johnson, H. L. 1963, Basic Astronomical Data, ed. K. Aa. Strand (Chicago: University of Chicago Press), p. 204.
Johnson, H. M. 1970, Ap. J. 160, 193.
_____ 1971, Ap. J. 164, 67.
Kerr, F. J. 1968, Nebulae and Interstellar Matter, ed. B. M. Middlehurst and L. H. Aller (Chicago: University of Chicago Press), p. 575.
Kerr, F. J. and Westerhout, G. 1965, in Galactic Structure, ed. A. Blaauw and M. Schmidt (Chicago: University of Chicago Press), p. 167.
Lang, K. R. 1971, Ap. J. 164, 249.
Lawrence, R. S. 1956, Ap. J. 123, 30.
Lerche, I. 1970, Astrophys. and Space Sci. 6, 287.
Lesh, J. R. 1968, Ap. J. Suppl. 17, 371.
Lilley, A. E. 1955, Ap. J. 121, 559.
Linblad, P. O. 1966, Bull. Ast. Inst. Netherlands Suppl. 1, 177.
McGee, R. X. and Milton, J. A. 1964, Australian J. Phys. 17, 128.
McGee, R. X., Milton, J. A. and Wolfe, W. 1966, Australian J. Phys., Astrophys. Suppl. No. 1, 3.
McGee, R. X. and Murray, J. D. 1961, Australian J. Phys. 14, 260.
McGee, R. X., Murray, J. D. and Milton, J. A. 1963, Australian J. Phys. 16, 136.
Menon, T. K. 1958, Ap. J. 127, 28.
Merrill, P. W., Sanford, R. F., Wilson, O. C. and Burwell, C. G. 1937, Ap. J. 86, 274.
Morton, D. C. 1967, Ap. J. 147, 1017.
Morton, D. C., Jenkins, E. B. and Brooks, N. H. 1969, Ap. J. 155, 875.
Muller, C. A. 1959, in Paris Symposium on Radio Astronomy, I.A.U. Symp. No. 9, ed. R. N. Bracewell (Stanford: Stanford University Press), p. 360.
Radhakrishnan, V., Murray, J. D. Lockhart, P. and Whittle, R. P. J. 1971, preprint.

Rodgers, A. W., Campbell, C. T., Whiteoak, J. B., Bailey, H. H. and Hunt, V. O. 1960, An Atlas of H-Alpha Emission in the Southern Milky Way (Canberra: Mount Stromlo Observatory).
Routly, P. M. and Spitzer, L., Jr. 1952, Ap. J. 115, 227.
Savage, B. D. and Code, A. D. 1970, in Ultraviolet Stellar Spectra and Related Ground-Based Observations, I.A.U. Symp. No. 36, ed. L. Houziaux and H. E. Butler (Dordrecht: D. Reidel Publ. Co.), p. 302.
Schmidt, M. 1957, Bull. Ast. Inst. Netherlands 13, 247.
Smith, A. M. 1969, Ap. J. 156, 93.
Spitzer, L., Jr. 1968, Diffuse Matter in Space (New York: Interscience), p. 67.
Spitzer, L., Jr., Epstein, I. and Hen, L. 1950, Ann. D' Ap. 13, 147.
Spitzer, L., Jr. and Zabriskie, F. R. 1959, Pub. A. S. P. 71, 412.
Stoeckly, R. and Dressler, K. 1964, Ap. J. 139, 240.
Strömgren, B. 1948, Ap. J. 108, 242.
Takakubo, K. 1967, Bull. Ast. Inst. Netherlands 19, 125.
Takakubo, K. and Van Woerden, H. 1966, Bull. Ast. Inst. Netherlands 18, 488.
Wampler, E. J. 1966, Ap. J. 144, 921.
Watanabe, K., Zelikoff, M. and Inn, E. C. Y. 1953, Absorption Coefficients of Several Atmospheric Gases, AFCRC Tech. Rep. No. 53-23.
Wiese, W. L., Smith, M. W. and Miles, B. M. 1969, Atomic Transition Probabilities, Vol. II (Washington: U. S. National Bureau of Standards).
Wisniewski, W. K. 1965, Sky and Telescope 30, 21.